Frequency-Domain Signal Processing for Spectrally-Enhanced CP-OFDM Waveforms in 5G New Radio

Juha Yli-Kaakinen, AlaaEddin Loulou, Toni Levanen, Kari Pajukoski, Arto Palin, Markku Renfors, *Life Fellow, IEEE*, and Mikko Valkama, *Senior Member, IEEE*

***Abstract*— Orthogonal frequency-division multiplexing (OFDM) has been selected as the basis for the fifth-generation new radio (5G NR) waveform developments. However, effective signal processing tools are needed for enhancing the OFDM spectrum in various advanced transmission scenarios. In earlier work, we have shown that fast-convolution (FC) processing is a very flexible and efficient tool for filtered-OFDM signal generation and receiver-side subband filtering, e.g., for the mixed-numerology scenarios of the 5G NR. FC filtering approximates linear convolution through effective fast Fourier transform (FFT)-based circular convolutions using partly overlapping processing blocks. However, with the continuous overlap-and-save and overlap-and-add processing models with fixed block-size and fixed overlap, the FC-processing blocks cannot be aligned with all OFDM symbols of a transmission frame. Furthermore, 5G NR numerology does not allow to use transform lengths shorter than 128 because this would lead to non-integer cyclic prefix (CP) lengths. In this article, we present new FC-processing schemes which solve or avoid the mentioned limitations. These schemes are based on dynamically adjusting the overlap periods and extrapolating the CP samples, which make it possible to align the FC blocks with each OFDM symbol, even in case of variable CP lengths. This reduces complexity and latency, e.g., in mini-slot transmissions and, as an example, allows to use 16-point transforms in case of a 12-subcarrier-wide subband allocation, greatly reducing the implementation complexity. On the receiver side, the proposed scheme makes it possible to effectively combine cascaded inverse and forward FFT units in FC-filtered OFDM processing. Transform decomposition is used to simplify these computations, leading to significantly reduced implementation complexity in various transmission scenarios. A very extensive set of numerical results is also provided, in terms of the radio-link performance and associated processing complexity.**

***Index Terms*— Filtered OFDM, multicarrier, waveforms, fast-convolution, physical layer, 5G, 5G new radio.**

Manuscript received June 12, 2020; revised November 28, 2020 and March 22, 2021; accepted April 26, 2021. Date of publication May 12, 2021; date of current version October 11, 2021. This work was supported in part by the Business Finland (formerly known as the Finnish Funding Agency for Innovation, Tekes) and Nokia Bell Labs through the Projects 5G-VIIMA and 5G-FORCE; in part by Nokia Networks; and in part by the Academy of Finland under Project 284694, Project 284724, and Project 319994. This article was presented in part at the Proceedings of Asilomar Conference on Signals, Systems, and Computers, Pacific Grove, California, USA [1]. The associate editor coordinating the review of this article and approving it for publication was D. So. *(Corresponding author: Juha Yli-Kaakinen.)*

Juha Yli-Kaakinen, Markku Renfors, and Mikko Valkama are with the Department of Electrical Engineering, Tampere University, 33101 Tampere, Finland (e-mail: juha.yli-kaakinen@tuni.fi; markku.renfors@tuni.fi; mikko.valkama@tuni.fi).

AlaaEddin Loulou, Toni Levanen, and Arto Palin are with Nokia Networks, 33100 Tampere, Finland (e-mail: alaaeddin.loulou@nokia.com; toni.a.levanen@nokia.com; arto.palin@nokia.com).

Kari Pajukoski is with Nokia Bell Labs, 90620 Oulu, Finland (e-mail: kari.pajukoski@nokia-bell-labs.com).

Color versions of one or more figures in this article are available at https://doi.org/10.1109/TWC.2021.3077762.

Data is available on-line at http://yli-kaakinen.fi/DiscontinuousSymbolSynchronizedFastConvolution/

Digital Object Identifier 10.1109/TWC.2021.3077762

I. Introduction

ORTHOGONAL frequency-division multiplexing (OFDM) is the dominating multicarrier modulation scheme and it is extensively deployed in modern radio access systems. OFDM offers high flexibility and efficiency in allocating spectral resources to different users through the division of subcarriers, simple and robust way of channel equalization due to the inclusion of cyclic prefix (CP), as well as simplicity of combining multi-antenna schemes with the core physical-layer processing [2]. The main drawback is the limited spectrum localization, especially in challenging new spectrum use scenarios like asynchronous multiple access, as well as mixed-numerology cases aiming to use adjustable symbol and CP lengths, subcarrier spacings (SCSs), and frame structures depending on the service requirements [3]–[7].

Various enhanced OFDM schemes have in general been proposed in the literature for solving the high out-of-band (OOB) emission problem. These include adaptive symbol transition [8], cancellation carriers [9], constellation expansion [10], polynomial cancellation coding [11], [12], subcarrier weighting [13], and precoding-based schemes [14], [15]. Two additional techniques, namely the time-domain windowing and subband- or carrier-level filtering [16], [17] are mainly considered in long-term evolution (LTE) and fifth-generation new radio (5G NR) context. To this end, the time-domain windowing with overlapping processing blocks, commonly referred to as weighted overlap-and-add (WOLA) in the 5G NR context, is a straightforward approach to sidelobe suppression by smoothing the discontinuities at the OFDM symbol boundaries [18]–[23]. This approach has a very low complexity and it can be applied also on the receiver (RX) side for suppressing interference leakage from adjacent channels. However, its effectiveness depends on the length of cyclic extensions of OFDM symbols, and there is an inevitable trade-off between sidelobe suppression performance and overhead in the throughput. The low complexity of WOLA makes it good alternative for user equipment (UE) side spectral control,

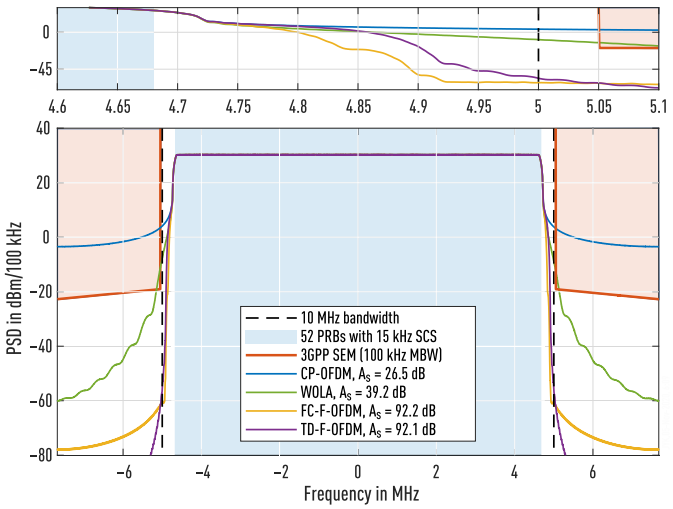

Fig. 1. Example PSDs of CP-OFDM, WOLA, FC-F-OFDM, and time-domain filtered OFDM (TD-F-OFDM) in 10 MHz 5G NR channel with 15 kHz SCS. The lower subfigure shows the overall responses while the upper subfigure shows the transition-band details. The PSDs are averaged with measurement bandwidth (MBW) of 100 kHz. The minimum attenuation at SEM mask edge, A_s, is given for each waveform.

however, meeting the strict base-station-side spectral emission mask (SEM) requirements of 3GPP and FCC with WOLA is challenging.

A. Filtered OFDM State-of-the-Art

Initial studies on filtered OFDM were based on time-domain filtering [24]–[26], and later also polyphase filter-bank-based solutions have been presented [22], [27]–[29]. Fast-convolution-based filtered OFDM (FC-F-OFDM) has been presented in [30]–[33]. Especially in [33], the flexibility, good performance, and low computational complexity of FC-F-OFDM was clearly demonstrated in the 5G NR context. These schemes typically apply filtering in continuous manner over a frame of CP-OFDM (or zero-prefix-OFDM) symbols.

An example PSD performance of CP-OFDM, WOLA, and frequency-domain and time-domain filtering-based CP-OFDM waveforms are shown in Fig. 1. As seen from this figure, the spectral containment of filtering-based enhanced-OFDM approaches is considerably better when compared to windowing-based WOLA. The problematic or inconvenient aspect of the conventional time-domain filtering-based schemes is their high complexity. In [34], it was shown that the complexity of time-domain filtering-based solutions in mixed-numerology case is 70 times the complexity of CP-OFDM processing. This complexity can be reduced using classical (e.g., polyphase) filter-bank models, however, these solutions have highly reduced flexibility in adjusting the subband center frequencies and bandwidths. Especially in 5G NR, where the subband size can, in theory, vary from one to 275 physical resource blocks (PRBs) and the center frequency of the subband can vary within a 100 MHz channel bandwidth, it is practically impossible to cover all possible subband sizes and center frequencies with a polyphase filter-bank implementation.

Universally filtered multicarrier (UFMC), also called universal filtered OFDM (UF-OFDM), is basically also a filtered-OFDM scheme, but it makes use of the zero prefix (ZP)-OFDM signal structure, instead of CP [35]. For UFMC, the filter length is basically limited by the ZP length which, e.g., for 5G NR numerologies, implies very short filters and, consequently, poor spectral containment. Also, ZP-based OFDM is not compatible with LTE and 5G NR physical layer standardization.

Yet another line of study is that of filter-bank multicarrier (FBMC) waveforms, which can reach excellent spectral localization. However, when targeting to maximize the spectrum utilization with FBMC, it is necessary to use offset quadrature amplitude modulation for subcarriers to reach orthogonality [36]. Due to the resulting inconveniences in the signal structure, the increase in computational complexity that FBMC entails, and the incompatibly with OFDM, its practical use has so far been limited to certain specific applications only. In addition, for FBMC waveforms, the excellent spectral localization implies poor time localization, making them unfeasible for short burst transmissions [34].

B. Contributions and Novelty

Building on our early work in [1], this article proposes and describes symbol-synchronized discontinuous FC processing targeting at increased flexibility and reduced complexity of FC-F-OFDM. It is shown that the proposed processing supports more flexible parametrization of the FC engine, resulting in reduced complexity and latency with narrow subband allocations and in mini-slot transmission. Important use cases are seen, e.g., in spectrally well-contained narrow-band internet-of-things (NB IoT) transmission with one PRB allocation and in ultra-reliable low-latency communications (URLLC) for generating short transmission bursts, so-called mini-slots, to reduce the radio link latency. However, the proposed schemes can be used for wide-band allocations as well.

Since FC is a block-wise processing scheme with fixed block length, the position of the useful parts of the OFDM symbols vary within a frame of transmitted OFDM symbols. With the continuous FC-processing model as described in [30], [33], it is necessary that the CP lengths and useful symbol durations correspond to an integer number of samples at the lower sampling rate used for transmitter OFDM processing at each subband. In case of narrow-band allocations, this limits the choice of the transform lengths, significantly increasing the computational complexity. With 3GPP LTE and 5G NR numerologies, the shortest possible transform length is 128, while length-16 transform would be sufficient when a subband contains one PRB (12 subcarriers) only. This restriction applies to plain CP-OFDM processing, time-domain filtering-based CP-OFDM, and FC-based solutions with continuous processing model. On the receiver side, the proposed scheme makes it possible to effectively combine cascaded inverse and forward fast Fourier transform (FFT) units in FC-filtered OFDM processing. Transform decomposition is used to simplify these computations, leading to significantly reduced implementation complexity in various transmission scenarios.

The proposed scheme allows to reduce the complexity in the case of (*i*) short transmissions (e.g. mini-slot), (*ii*) in multiplexing multiple relatively narrow subbands (e.g., gateway for massive machine-type communications (MTC)), and (*iii*) UE side transmitter (TX) processing, assuming that only one numerology is transmitted. Moreover, in case of parallelized hardware implementations, it is a benefit that each OFDM symbol can be generated and filtered independently of the others. This also minimizes the TX signal processing latency.

In this article, we develop and describe discontinuous symbol-synchronized FC-based processing techniques, with emphasis on exact mathematical descriptions and the corresponding insight in the involved processing stages. The main contributions can be listed and summarized as follows:

- Mathematical models for discontinuous symbol-synchronized FC-based TX and RX processing are described. Both overlap-and-add (OLA) and overlap-and-save (OLS) variants are discussed.
- Extrapolating TX FC processing is suggested for reducing the required inverse fast Fourier transform (IFFT) length for OFDM modulation by relaxing the CP length related constraints on the IFFT length.
- Model for simplifying the IFFT computations in RX processing is proposed. The computational savings are achieved by effectively combining the computations of the IFFT of the FC module and the FFT of subband OFDM processing through transform decomposition.
- Extensive numerical results are provided, including comprehensive 5G NR radio link simulations, verifying the validity of the proposed models, and illustrating the benefits of the proposed FC-based filtered-OFDM processing.
- Complexity evaluations are given quantifying the savings achieved using the proposed techniques.
- Discontinuous FC processing is proposed as an additional useful element in the toolbox for frequency-domain waveform processing, and it can be expected to find applications also in other areas of digital signal processing.

The remainder of this paper is organized as follows. Section II, first shortly reviews the continuous FC-based filtered-OFDM processing, for reference. Then, the proposed discontinuous TX FC-processing model is described with implementation alternatives resulting to the reduced complexity and latency in Section III for TX and in Section IV for RX. Section V presents an analysis of the computational complexity of considered alternative FC schemes. In Section VI, the performance of the discontinuous processing is analyzed in terms of uncoded bit error rate (BER) in different interference/multiplexing scenarios and channel conditions, while also numerical results for the complexity for alternative FC schemes are provided. Finally, the conclusions are drawn in Section VII.

II. Continuous Fast-Convolution Processing

A. Basic Operation Principle

The block diagram for the basic continuous, symbol-nonsynchronized OLA-based FC-F-OFDM TX processing proposed originally in [30], [33], serving as the main state-of-the-art reference, is shown in Fig. 2. Let us denote by $L_{\text{act},m}$ the number of active subcarriers on subband m. The CP-OFDM signal is first generated by using the smallest IFFT length equal to or larger than $L_{\text{act},m}$ supporting an integer length CP. Let us denote this transform (IFFT) length by $L_{\text{OFDM},m}$. Then, low-rate CP of length $L_{\text{CP},m,n}$ is added to each of the $B_{\text{OFDM},m}$ OFDM symbols for $n = 0, 1, \ldots, B_{\text{OFDM},m} - 1$ and the signal is converted to serial format. These are all operations equivalent to basic CP-OFDM TX processing.

The actual FC processing per subband starts by partitioning the time-domain input sample stream into so-called FC processing blocks, which include overlapping zero-padded extensions, as illustrated in Fig. 3. Here, the basic idea is to approximate linear convolution through series of overlapping circular convolutions carried out per FC processing block. The exact number of these blocks depends on the input sequence length, overlap factor, and the FFT length L_m. Next, we take L_m-point FFT of each processing block and apply FFT-shift operation which essentially places the DC-carrier in the middle of each vector. Then, a frequency-domain window $\mathbf{D}_m$ is applied to implement the designed filter response. After frequency-domain windowing the given subband is placed at the allocated FFT bins with transition-band values possibly exceeding the nominal allocation range. The overlapping transition-band bins of adjacent subbands are added together finalizing the subband-wise processing.

The N-point IFFT is common part for all subbands. It converts all the low-rate frequency-division multiplexed subband signals to time domain per FC block. By using the common IFFT block for all subbands, the complexity of processing can be considerably reduced. In addition, it provides the sampling-rate conversion by the factor of $I_m = N/L_m$. Next, OLA processing is used to concatenate the high-rate FC blocks in order to construct the filtered time-domain representation of the transmitted signal.

In addition to OLA approach, FC processing can be realized using OLS scheme. In this case, the zero padding in block partitioning is replaced by the straightforward segmentation into the overlapping blocks and the OLA after the last transform is replaced by the discarding of the overlapping output segments. More detailed description of the FC filtering process can be found, e.g., from [33], [37].

The basic continuous FC-processing flow of FC-F-OFDM transmitter for $L_{\text{OFDM},m} = L_m$ is illustrated in Fig. 3. We use mini slot of two OFDM symbols ($B_{\text{OFDM},m} = 2$) as an example to illustrate our point of more efficient processing of short symbol bursts with the discontinuous processing defined in the next section. The assumed overlap between processing blocks is 50% (the overlap factor is $\lambda = 0.5$). From Fig. 3 we can observe how the FC processing is continuous by collecting $L_{\text{OFDM},m}/2 = L_m/2$ samples from the input sample stream to each FC processing block. Also, the overlap factor is constant over all FC processing blocks.

The inconvenient aspects of the original continuous FC processing in the considered short burst transmission scenario are threefold: First, there is inherent latency in processing flow since each FC processing block may contain samples of two OFDM symbols. For example, the filtering of the first OFDM

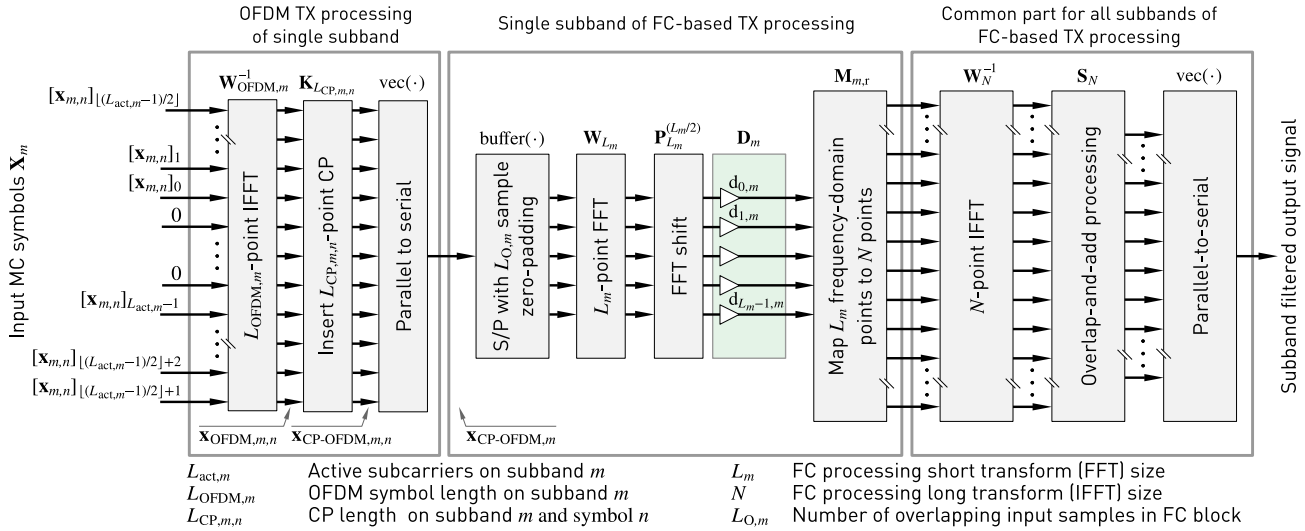

Fig. 2. Block diagram of basic FC-F-OFDM transmitter processing using the OLA model. Some essential notations are clarified here for reference.

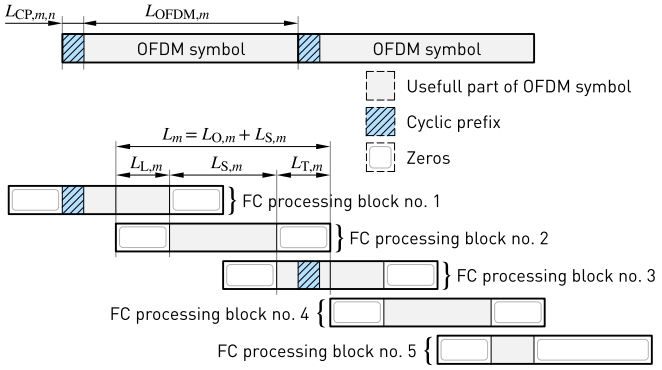

Fig. 3. FC-processing block partitioning in basic continuous OLA-based FC-F-OFDM. FC blocks are not synchronized to CP-OFDM symbols. Five FC-processing blocks are needed for two OFDM symbols.

symbol cannot be finalized until the second OFDM symbol in the third FC processing block is available as illustrated Fig. 3. Second, the number of required FC processing blocks is somewhat higher, e.g., the fifth FC block is almost empty making processing inefficient. This "extra" overhead of the continuous FC processing, however, decreases with increasing number of OFDM symbols, or increased length of transmitted signal. Third, the OFDM transform lengths supported by the continuous FC processing, or any other continuous filtering alternative, are restricted by the CP length requirement, often making the processing excessively complex for narrow-band allocations.

B. Continuous FC-Filtered CP-OFDM TX Processing Model

The CP-OFDM TX processing, as illustrated in left-hand side block in Fig. 2, is formally expressed as

$$\mathbf{x}_{\mathrm{OFDM},m,n} = \mathbf{W}^{-1}_{L_{\mathrm{OFDM},m}} \mathbf{x}_{m,n} \tag{1a}$$

and

$$\mathbf{x}_{\mathrm{CP\text{-}OFDM},m,n} = \mathbf{K}_{L_{\mathrm{CP},m,n}} \mathbf{x}_{\mathrm{OFDM},m,n}, \tag{1b}$$

where $\mathbf{x}_{m,n} \in \mathbb{C}^{L_{\mathrm{OFDM},m}\times 1}$ is the vector containing the incoming quadrature amplitude modulation (QAM) symbols on $L_{\mathrm{act},m}$ active subcarriers, $\mathbf{W}^{-1}_{L_{\mathrm{OFDM},m}} \in \mathbb{C}^{L_{\mathrm{OFDM},m}\times L_{\mathrm{OFDM},m}}$ is the unitary inverse discrete Fourier transform (IDFT) matrix (i.e., $\mathbf{W}\mathbf{W}^* = \mathbf{I}$), and $\mathbf{K}_{L_{\mathrm{CP},m,n}} \in \mathbb{Z}^{(L_{\mathrm{OFDM},m}+L_{\mathrm{CP},m,n})\times L_{\mathrm{OFDM},m}}$ is the CP insertion matrix. In general, the CP length could be different for each symbol, while for 5G NR and LTE, two CP lengths are used for normal CP configuration [38], [39] such that the first symbol of a half subframe (0.5 ms) is longer than the others. For example, with $L_{\mathrm{OFDM},m} = 128$, the CP length for the first symbol in a half subframe is $L_{\mathrm{CP},m,n} = 10$ for $n \bmod 7 = 0$ and $L_{\mathrm{CP},m,n} = 9$, otherwise.

FC-based filtering, as proposed originally in [30], [33], carries out the processing in overlapping blocks. In the synthesis filter bank (SFB) case, the input block length of the mth subband is L_m and the output block length is N. The overlap between the input blocks is determined by the number of overlapping input samples $L_{\mathrm{O},m}$. The number of non-overlapping input samples is given as $L_{\mathrm{S},m} = L_m - L_{\mathrm{O},m}$ while the overlap factor is expressed using these values as

$$\lambda = L_{\mathrm{O},m}/L_m = (L_m - L_{\mathrm{S},m})/L_m. \tag{2}$$

The number of overlapping input samples can be further divided into leading and tailing overlapping parts as follows:

$$L_{\mathrm{L},m} = \lceil L_{\mathrm{O},m}/2 \rceil \quad \text{and} \quad L_{\mathrm{T},m} = \lfloor L_{\mathrm{O},m}/2 \rfloor. \tag{3}$$

The corresponding number of overlapping and non-overlapping output samples are determined as $N_{\mathrm{O}} = \lambda N$ and $N_{\mathrm{S}} = (1-\lambda)N$, respectively. Similarly, the number of overlapping output samples are divided into leading and tailing parts, N_{L} and N_{T}, respectively.

The FC processing increases the sampling rate by the factor of

$$I_m = N/L_m, \tag{4}$$

resulting in OFDM symbol and CP durations of $N_{\text{OFDM},m} = I_m L_{\text{OFDM},m}$ and $N_{\text{CP},m,n} = I_m L_{\text{CP},m,n}$, respectively. Here $L_{\text{OFDM},m}$ and $L_{\text{CP},m,n}$ must have integer values.

In continuous FC SFB, the filtering of the mth CP-OFDM subband signal for the generation of the high-rate waveform $\mathbf{w}_m$ can be represented as

$$\mathbf{w}_m = \mathbf{F}_m \begin{bmatrix} \mathbf{0}_{(L_m - L_{\text{S},m})\times 1} \\ \mathbf{x}_{\text{CP-OFDM},m} \\ \mathbf{0}_{(L_m - L_{\text{S},m} + V_m)\times 1} \end{bmatrix}, \tag{5a}$$

where $\mathbf{F}_m$ is the block diagonal transform matrix of the form

$$\mathbf{F}_m = \text{diag}(\mathbf{F}_{m,0}(\varphi_{m,0}), \mathbf{F}_{m,1}(\varphi_{m,1}), \ldots, \mathbf{F}_{m,R_m-1}(\varphi_{m,R_m-1})) \tag{5b}$$

with R_m overlapping blocks $\mathbf{F}_{m,r}(\varphi_{m,r}) \in \mathbb{C}^{N\times L_m}$ for $r = 0, 1, \ldots, R_m - 1$. Here, $\mathbf{x}_{\text{CP-OFDM},m}$ is the column vector formed by concatenating the $\mathbf{x}_{\text{CP-OFDM},m,n}$ for $n = 0, 1, \ldots, B_{\text{OFDM},m} - 1$. In order to properly segment the beginning and the end of the input stream with OLS or OLA scheme, zero padding of $S_{\text{L},m} = 2(L_m - L_{\text{S},m}) + V_m$ samples in total are inserted before and after the CP-OFDM signal, where V_m is the number of samples needed to fill the non-overlapping part of the last FC processing block. The overall high-rate waveform to be transmitted is then obtained by combining all the subband waveforms as follows:

$$\mathbf{x}_{\text{FC-F-OFDM}} = \sum_{m=0}^{M-1} \mathbf{w}_m. \tag{6}$$

The multirate version of the FC SFB can be represented either using the OLA block processing by decomposing the $\mathbf{F}_{m,r}(\varphi_{m,r})$'s as the following matrix

$$\mathbf{F}^{(\text{OLA})}_{m,r}(\varphi_{m,r}) = \mathbf{W}_N^{-1}\mathbf{M}_m(\varphi_{m,r})\mathbf{D}_m\mathbf{P}^{(L_m/2)}_{L_m}\mathbf{W}_{L_m}\mathbf{A}^{(\text{TX})}_{m,r} \tag{7a}$$

or OLS block processing when the $\mathbf{F}_{m,r}(\varphi_{m,r})$'s are decomposed as

$$\mathbf{F}^{(\text{OLS})}_{m,r}(\varphi_{m,r}) = \mathbf{S}^{(\text{TX})}_{m,r}\mathbf{W}_N^{-1}\mathbf{M}_m(\varphi_{m,r})\mathbf{D}_m\mathbf{P}^{(L_m/2)}_{L_m}\mathbf{W}_{L_m}. \tag{7b}$$

Here, $\mathbf{W}_{L_m} \in \mathbb{C}^{L_m\times L_m}$ and $\mathbf{W}_N^{-1} \in \mathbb{C}^{N\times N}$ are unitary discrete Fourier transform (DFT) and IDFT matrices, respectively. The DFT shift matrix $\mathbf{P}^{(L_m/2)}_{L_m} \in \mathbb{N}^{L_m\times L_m}$ is circulant permutation matrix, as expressed by

$$\mathbf{P}^{(L_m/2)}_{L_m} = \begin{bmatrix} \mathbf{0}_{\lfloor L_m/2\rfloor\times\lceil L_m/2\rceil} & \mathbf{I}_{\lfloor L_m/2\rfloor} \\ \mathbf{I}_{\lceil L_m/2\rceil} & \mathbf{0}_{\lceil L_m/2\rceil\times\lfloor L_m/2\rfloor} \end{bmatrix}, \tag{8}$$

placing the zero-frequency bin in the middle of the frequency-domain representation of the waveform while $\mathbf{D}_m \in \mathbb{R}^{L_m\times L_m}$ is diagonal matrix with diagonal elements being the weights of the subband m. The frequency-domain mapping matrix $\mathbf{M}_m(\varphi_{m,r}) \in \mathbb{N}^{N\times L_m}$ maps L_m consecutive frequency-domain bins of the input signal to L_m consecutive frequency-domain bins of the output signal as follows:

$$[\mathbf{M}_m(\varphi_{m,r})]_{q,p} = \begin{cases} \varphi_{m,r}, & \text{if } \Xi(p) = q \\ 0, & \text{otherwise} \end{cases} \tag{9a}$$

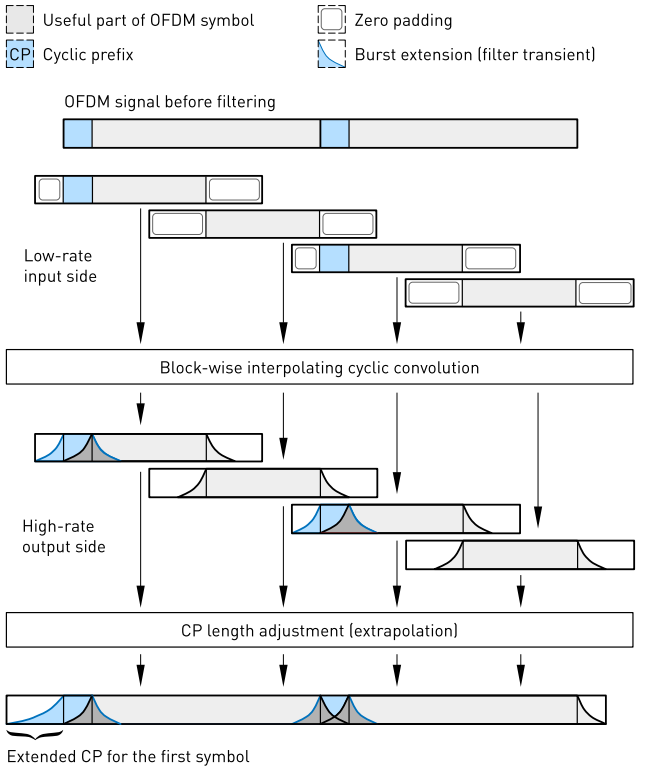

Fig. 4. Discontinuous OLA-based block partitioning for FC-F-OFDM TX processing. FC processing blocks are synchronized to the OFDM symbols. Four FC-processing blocks are needed for two OFDM symbols. The FC overlap factor is dynamic: $0.5 - N_{\text{CP},n}/N$ for the first block and 0.5 for the second block of each OFDM symbol.

with

$$\Xi(p) = (c_m - \lceil L_m/2\rceil + p - 1 \bmod N) + 1, \tag{9b}$$

where c_m is the center bin of the subband m. In other words, $\mathbf{M}_m(\varphi_{m,r})$ provides frequency translation or modulation by shifting the L_m bins in frequency domain by c_m bins. The phase rotation needed to maintain the phase continuity between the consecutive overlapping processing blocks is given as

$$\varphi_{m,r} = \exp(\text{j}2\pi r c_m L_{\text{S},m}/L_m). \tag{9c}$$

For further details, see [33].

For OLA processing, the time-domain analysis window matrix $\mathbf{A}_{m,r} \in \mathbb{N}^{L_m\times L_m}$ is a diagonal weighting matrix as given by

$$\mathbf{A}^{(\text{TX})}_{m,r} = \text{diag}\,(\mathbf{a}_{m,r}) \quad \text{with} \quad \mathbf{a}_{m,r} = \begin{bmatrix} \mathbf{0}_{L_{\text{L},m}\times 1} \\ \mathbf{1}_{L_{\text{S},m}\times 1} \\ \mathbf{0}_{L_{\text{T},m}\times 1} \end{bmatrix}. \tag{10a}$$

For OLS processing, the time-domain synthesis window matrix $\mathbf{S}_{m,r} \in \mathbb{N}^{N\times N}$ is given by

$$\mathbf{S}^{(\text{TX})}_{m,r} = \text{diag}\,(\mathbf{s}_{m,r}) \quad \text{with} \quad \mathbf{s}_{m,r} = \begin{bmatrix} \mathbf{0}_{N_{\text{L}}\times 1} \\ \mathbf{1}_{N_{\text{S}}\times 1} \\ \mathbf{0}_{N_{\text{T}}\times 1} \end{bmatrix}. \tag{10b}$$

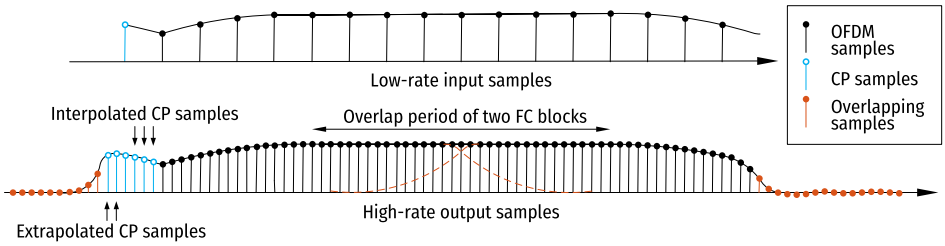

Fig. 5. Discontinuous OLA processing for a single CP-OFDM symbol with 50% FC overlap, interpolation factor of four ($I_m = 4$), and high-rate OFDM symbol duration of 64 samples. CP length is one sample at low rate and six samples at high rate (corresponding to one and half low-rate samples).

III. Proposed Symbol-Synchronized Discontinuous FC-Based Filtered-OFDM TX Processing

A. Basic Idea and Operating Principle

Fig. 4 illustrates the proposed discontinuous TX FC-F-OFDM processing flow for a mini-slot of two OFDM symbols ($B_{\mathrm{OFDM},m} = 2$). Here, the block segmentation of the discontinuous FC processing is specifically tailored to follow the OFDM waveform structure by dynamically adjusting the overlap between the FC blocks. It can be seen that in discontinuous processing, two FC processing blocks are synchronized to each OFDM symbol. With the chosen parameters, the first FC block contains the first half of the OFDM symbol and the second FC block contains the second half of the OFDM symbol. In addition, the first FC processing block contains the low-rate CP samples. This reduces the overlap in the beginning of the first FC block, that is, the overlap factor becomes $\lambda = 0.5 - L_{\mathrm{CP},m,n}/L_m$. Here, $L_{\mathrm{CP},m,n}$ is the CP length of the nth symbol on subband m. In practice, this reduction is relatively small, causing only minor increase in the related distortion effects which do not essentially contribute to link level performance. For discontinuous processing, only four FC processing blocks are used, instead of five in the continuous processing model (see Fig. 3), resulting in reduced complexity. For longer transmission bursts, the discontinuous processing systematically requires one or two FC processing blocks less than the continuous one. Obviously, the segmentation can also be carried out, e.g., by dividing the CP-OFDM symbol into two segments such that these segments have equal length in both FC processing blocks (assuming that the CP length is even). However, for the proposed approach, the payload part of symbol is better protected by the reduced overlap since the increased cyclic distortion falls above the CP part of the symbol.

Fig. 5 shows a detailed example of the sample-level interpolation and extrapolation process. The CP part is included in the leading overlap section of the first FC block of each OFDM symbol and the CP length is fine-tuned in the OLA processing for consecutive OFDM symbols at high rate. The time resolution in adjusting the CP length is equal to the sampling interval at high rate (as in traditional CP-OFDM).

In generic setting, the discontinuous FC-F-OFDM process can be formulated as follows. First, the CP-OFDM symbols are generated at the minimum feasible sampling rate for each subband and, if needed, the CP length is truncated to the highest integer number of low-rate samples which does not exceed the CP length of the transmitted signal. FC-based filtering (or interpolation) is then applied to each CP-OFDM symbol individually to generate filtered symbols at the high (output) sampling rate. Finally, the CP-OFDM signal for a transmission slot is constructed from the generated individual symbols using the OLA principle. When combining the individual symbols, their spacing in time direction is adjusted (with the precision of the output sampling interval) to correspond to the precise CP duration in the "CP length adjustment (extrapolation)" block in Fig. 4.

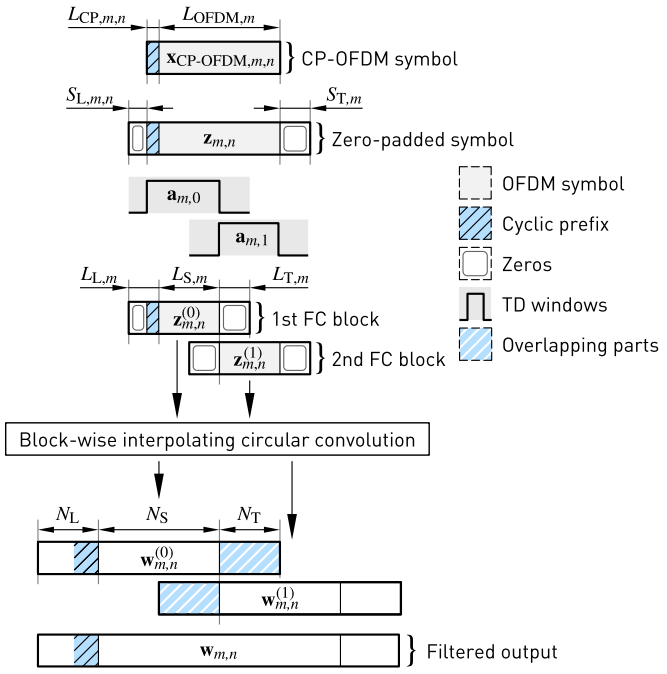

Fig. 6. Overlap-and-add (OLA)-based block processing of one CP-OFDM symbol using two FC-processing blocks.

In basic form, the proposed scheme is suitable for scenarios where the overall symbol durations of all subband signals to be transmitted have equal lengths and the symbols are synchronized. It is notable that different durations (e.g., different CP lengths) are allowed for different CP-OFDM symbol intervals within a transmission slot.

B. Symbol-Synchronized TX FC Processing for One CP-OFDM Symbol

Fig. 6 illustrates the OLA-based FC processing of one CP-OFDM symbol in two processing blocks corresponding

to overlap factor of $\lambda = 0.5$. Here, it is assumed that the OFDM modulation IFFT lengths and the FC-processing short transform (FFT) lengths are the same, that is, $L_{\mathrm{OFDM},m} = L_m$ for $m = 0, 1, \ldots, M-1$. This is due to the fact, that some additional simplifications especially on RX can be provided if $L_m = L_{\mathrm{OFDM},m}$ and the FC processing with overlap of (about) 50% has turned out to provide sufficient performance for LTE and 5G NR channelization purposes. However, the proposed scheme can be generalized for other overlap factors and transform lengths as well if desired.

In symbol-synchronized processing, the incoming symbol is first zero padded in the beginning and the end by $S_{\mathrm{L},m,n} = L_{\mathrm{L},m} - L_{\mathrm{CP},m,n}$ and $L_{\mathrm{T},m}$ zeros, respectively, to form a zero-padded symbol $\mathbf{z}_{m,n}$ of length $3/2L_m$ as follows

$$\mathbf{z}_{m,n} = \begin{bmatrix} \mathbf{0}_{S_{\mathrm{L},m,n} \times (L_{\mathrm{OFDM},m} + L_{\mathrm{CP},m,n})} \\ \mathbf{I}_{L_{\mathrm{OFDM},m} + L_{\mathrm{CP},m,n}} \\ \mathbf{0}_{L_{\mathrm{T},m} \times (L_{\mathrm{OFDM},m} + L_{\mathrm{CP},m,n})} \end{bmatrix} \mathbf{x}_{\text{CP-OFDM},m,n}. \quad (11)$$

This zero padding is needed in order to divide one CP-OFDM symbol of length $L_{\mathrm{CP},m,n} + L_{\mathrm{OFDM},m}$ into the two FC blocks of length L_m with 50% overlap. Now $\mathbf{F}_{m,r}(\varphi_{m,r})$'s for $r = 0, 1$, (e.g., the synthesis matrix of (7a)) essentially process (filter and possibly interpolate) two overlapping segments of length L_m from the zero-padded symbol. Let us denote these segments by $\mathbf{z}_{m,n}^{(r)} \in \mathbb{C}^{L_m \times 1}$ for $r = 0, 1$ and the samples belonging to these processing segments are given by

$$\mathbf{z}_{m,n}^{(r)} = (\mathbf{R}_{L_m}^{(r)})^{\mathsf{T}} \mathbf{z}_{m,n} \quad (12a)$$

for $r = 0, 1$ where

$$\mathbf{R}_{L_m}^{(0)} = \begin{bmatrix} \mathbf{I}_{L_m} \\ \mathbf{0}_{L_m/2 \times L_m} \end{bmatrix} \quad \text{and} \quad \mathbf{R}_{L_m}^{(1)} = \begin{bmatrix} \mathbf{0}_{L_m/2 \times L_m} \\ \mathbf{I}_{L_m} \end{bmatrix}. \quad (12b)$$

The effective overlap factor for the first processing block is reduced to $0.5 - L_{\mathrm{CP},m,n}/L_m$ due to inclusion of CP and, therefore, the first time-domain analysis window has to be redefined as

$$\mathbf{a}_{m,0} = \begin{bmatrix} \mathbf{0}_{S_{\mathrm{L},m,n} \times 1} \\ \mathbf{1}_{(L_{\mathrm{S},m} + L_{\mathrm{CP},m,n}) \times 1} \\ \mathbf{0}_{L_{\mathrm{T},m} \times 1} \end{bmatrix} \quad (13)$$

in order to prevent CP samples being zeroed by the analysis window of (10a). Let $\mathbf{w}_{m,n}^{(r)} \in \mathbb{C}^{N \times 1}$ for $r = 0, 1$ denote the product of the processing blocks by the synthesis matrices as expressed by

$$\mathbf{w}_{m,n}^{(r)} = \mathbf{F}_{m,r}(\varphi_{m,r}\theta_n)\mathbf{z}_{m,n}^{(r)} \quad (14a)$$

for $r = 0, 1$. Here, an additional phase rotation as given by

$$\theta_n = \exp(\mathrm{j}2\pi c_m \varphi_n) \quad (14b)$$

with

$$\varphi_n = \frac{1}{N} \sum_{q=1}^{n} N_{\mathrm{CP},m,q}, \quad (14c)$$

is included to compensate the truncation of the CP length to integer samples on the low-rate side. This additional phase rotation is included to guarantee the phase continuity of the signal segments generated in the following OLA stages.

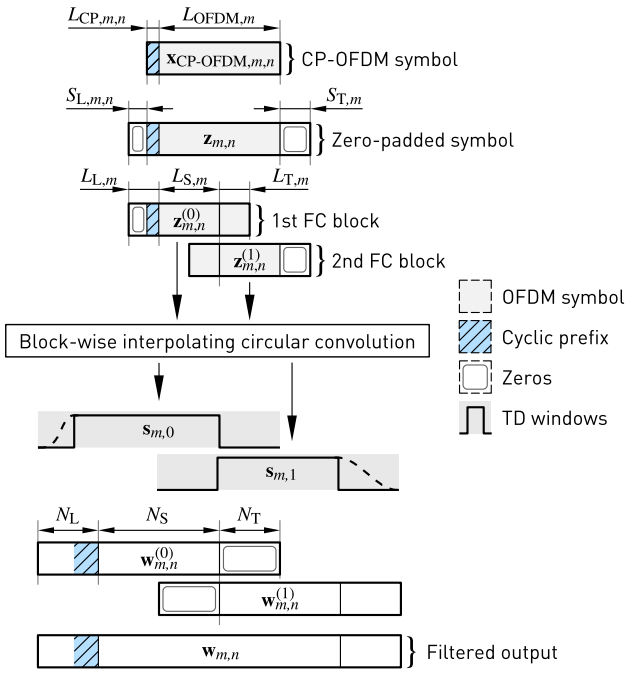

Fig. 7. Overlap-and-save (OLS)-based block processing of one CP-OFDM symbol using two FC-processing blocks.

The filtered high-rate subband waveform of length $3/2N$ corresponding the nth symbol on the mth subband can finally obtained be combining these filtered blocks by following the OLA scheme as

$$\mathbf{w}_{m,n} = \sum_{r=0,1} \mathbf{R}_N^{(r)} \mathbf{w}_{m,n}^{(r)} \quad (15a)$$

where

$$\mathbf{R}_N^{(0)} = \begin{bmatrix} \mathbf{I}_N \\ \mathbf{0}_{N/2 \times N} \end{bmatrix} \quad \text{and} \quad \mathbf{R}_N^{(1)} = \begin{bmatrix} \mathbf{0}_{N/2 \times N} \\ \mathbf{I}_N \end{bmatrix}. \quad (15b)$$

Alternative to OLA scheme, the above processing can also be carried out following the OLS approach as illustrated in Fig. 7. The basic difference is that now the time-domain windowing is realized after the convolution and only one of the filtered blocks is non-zero in the overlapping regions. The abrupt truncation of output waveform at the edges of the filtered symbol can be avoided by smoothly tapering the raising edge of the first time-domain synthesis window $\mathbf{s}_{m,0}$ and the falling edge of the second time-domain window $\mathbf{s}_{m,1}$, as illustrated using the dashed line in Fig. 7. Discontinuities in the output waveform give raise to a high spectral leakage and, therefore, the OLA scheme is preferable on the TX side in general.

C. Symbol-Synchronized TX FC Processing for Multiple Symbols

The final stage of the proposed discontinuous FC processing consists of combining the filtered CP-OFDM symbols, provided that more than one symbol is included in the transmission slot. In this case, the high-rate filtered symbols are

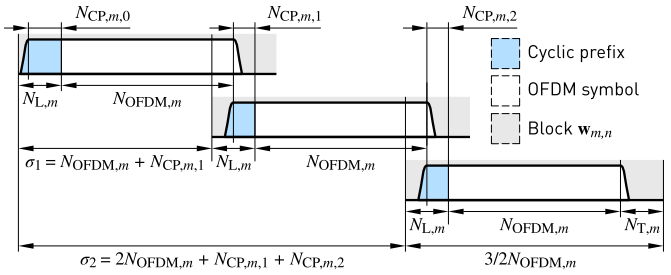

Fig. 8. Symbol-wise overlap-and-add processing for concatenating the filtered CP-OFDM symbols.

combined with symbol-wise OLA processing as follows

$$\mathbf{w}_m = \sum_{n=0}^{B_{\text{OFDM},m}-1} \mathbf{\Gamma}_{\sigma_n} \mathbf{w}_{m,n} \tag{16a}$$

with

$$\sigma_n = nN_{\text{OFDM},m} + \sum_{q=1}^{n} N_{\text{CP},m,q} \tag{16b}$$

being the starting index of the nth filtered block $\mathbf{w}_{m,n}$ of length $3/2N_{\text{OFDM},m}$ in $\mathbf{w}_m$ as illustrated in Fig. 8. Here, Q-by-$3/2N$ matrix

$$\mathbf{\Gamma}_p = \begin{bmatrix} \mathbf{0}_{p\times 3/2N} \\ \mathbf{I}_{3/2N} \\ \mathbf{0}_{(Q-3/2N-p)\times 3/2N} \end{bmatrix} \tag{16c}$$

with

$$Q = N_{\text{L},m} + N_{\text{T},m} + B_{\text{OFDM},m}N_{\text{OFDM},m} + \sum_{n=1}^{B_{\text{OFDM},m}-1} N_{\text{CP},m,n} \tag{16d}$$

aligns the filtered symbols to their desired time-domain locations at the high-rate output sequence. In other words, the filtered CP-OFDM symbols are aligned in time direction such that the transmitted stream of the symbols can be received by using a plain CP-OFDM RX without any additional processing.

D. CP Extrapolation by TX FC Processing

Suppose that $L_{\text{OFDM},m}$ is chosen such that the CP length on the low-rate side is not an integer, that is, $L_{\text{OFDM},m} < 128$ for 5G NR and LTE numerologies. In this case, CP length can be rounded to next smaller integer as given by

$$L_{\text{CP},m,n} = \lfloor N_{\text{CP},m,n}/I_m \rfloor \tag{17}$$

and the FC-based filtering with the accompanying symbol-wise overlap-and-add processing as given by (16) inherently extrapolates $N_{\text{CP},m,n} - N/L_m L_{\text{CP},m,n}$ samples at the high-rate side corresponding to fractional part of the low-rate CP, as illustrated in Fig. 5.

As an example, in the 10 MHz 5G NR or LTE case with 15 kHz SCS and normal CP length, the output sampling rate is $f_{\text{s,out}} = 15.36$ MHz, the useful OFDM symbol duration is

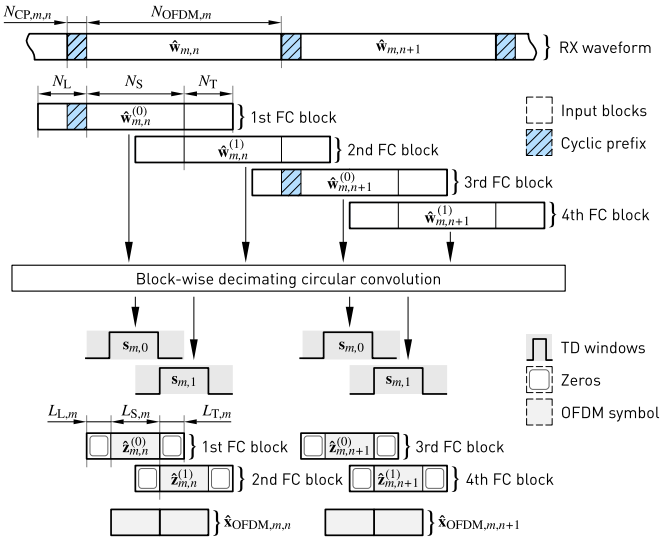

Fig. 9. Discontinuous OLS processing for FC-F-OFDM receiver with overlap factor of $\lambda = 0.5$. FC processing blocks are synchronized to the OFDM symbols. Four FC-processing blocks are needed for two OFDM symbols.

$N_{\text{OFDM},m} = 1024$ high-rate samples, and the CP length is $N_{\text{CP},m,n} = 80$ high-rate samples for the first symbol (for $n \bmod 7 = 0$) of each slot of 7 symbols, and $N_{\text{CP},m,n} = 72$ samples for the others (for $n \bmod 7 \neq 0$). Then in the continuous processing model, the smallest possible OFDM IFFT length is $L_{\text{OFDM},m} = 128$, corresponding to $f_{\text{s,in}} = 1.92$ MHz input sampling rate, and the CP lengths are $L_{\text{CP},m,n} = 10$ and $L_{\text{CP},m,n} = 9$ low-rate samples for the first and other symbols, respectively. However, using the discontinuous FC processing model with narrow subband allocations, like 12, 24, or 48 subcarriers (SCs), the OFDM IFFT length $L_{\text{OFDM},m}$ can be reduced to 16, 32, or 64, respectively. These transform lengths correspond at the low-rate side to CP lengths, $L_{\text{CP},m,n}$, of 1.25, 2.5, and 5.0 samples for the first symbol or 1.125, 2.25, and 4.5 samples for the others. The same transform (IFFT) lengths are used for the subband OFDM signal generation.

One important case is NB IoT using 180 kHz transmission bandwidth corresponding to a single PRB (12 SCs) and needing IFFT of length $L_{\text{OFDM},m} = 128$ and input sampling rate of $f_{\text{s,in}} = 1.92$ MHz in traditional implementation. Discontinuous processing allows to generate the signal by using the FFT length of 16 for the OFDM symbol generation and FC processing at the input sampling rate of $f_{\text{s,in}} = 16/128 \times 1.92$ MHz $=$ 240 kHz.

IV. Symbol-Synchronized Discontinuous FC-Based Filtered-OFDM RX Processing

As for the TX side, the basic continuous FC-processing flow of FC-F-OFDM RX requires five FC-processing blocks in order to process two CP-OFDM symbols. In this case, the CPs are discarded after the FC filtering as part of normal RX CP-OFDM reception. With continuous processing, the FC-processing chain needs to wait for varying number of samples belonging to the second OFDM symbol before it can start processing the third FC-processing block in order to

obtain final samples in the output for the first OFDM symbol. In discontinuous processing, as seen in Fig. 9, the RX waits only for the samples belonging to the first OFDM symbol and desired amount of overlapping samples from the beginning of the second symbol, after which it can start processing the second FC processing block, providing at the output the last filtered samples of the first OFDM symbol. This allows to provide constant delay for RX processing and also can lead to reduced buffering requirements in the RX.

In the case of maximal timing-adjustment flexibility, the number of samples collected from the following CP-OFDM symbol corresponds to the number of overlapping samples at the end of FC processing block. In addition, in discontinuous processing, two first FC processing blocks can be processed independently from the two following FC processing blocks, as they represent different OFDM symbols. In continuous processing, two OFDM symbols are linked through common samples in the third FC processing block.

Because the content (FC block contains first or second half of OFDM symbol) and processing of even and odd FC processing blocks remain constant over the whole RX signal, we can process even and odd blocks separately from each other. This allows for an implementation where even and odd FC processing blocks are processed in parallel FC processing chains, allowing to minimize the latency of the RX implementation.

Due to the orthogonality, the analysis matrix on the RX side is the conjugate transpose of the synthesis matrix on the TX side [40]. Furthermore, since the order of the operations in the transposition is reversed, the OLS scheme on the TX side becomes the OLA scheme on the RX side and vice versa. Thus, the analysis matrix for the OLS and OLA schemes are given as

$$\begin{aligned}\mathbf{G}_{m,r}^{(\mathrm{OLS})}(\varphi_{m,r}) &= \mathbf{F}_{m,r}^{(\mathrm{OLA})}(\varphi_{m,r})^{\mathsf{H}} \\ &= \left(\mathbf{W}_N^{-1}\mathbf{M}_m(\varphi_{m,r})\mathbf{D}_m\mathbf{P}_{L_m}^{(L_m/2)}\mathbf{W}_{L_m}\mathbf{A}_{m,r}^{(\mathrm{TX})}\right)^{\mathsf{H}} \\ &= \mathbf{S}_{m,r}^{(\mathrm{RX})}\mathbf{W}_{L_m}^{-1}\mathbf{P}_{L_m}^{(-L_m/2)}\mathbf{D}_m\mathbf{M}_m(\varphi_{m,r})^{\mathsf{T}}\mathbf{W}_N \end{aligned} \tag{18a}$$

and

$$\begin{aligned}\mathbf{G}_{m,r}^{(\mathrm{OLA})}(\varphi_{m,r}) &= \mathbf{F}_{m,r}^{(\mathrm{OLS})}(\varphi_{m,r})^{\mathsf{H}} \\ &= \mathbf{W}_{L_m}^{-1}\mathbf{P}_{L_m}^{(-L_m/2)}\mathbf{D}_m\mathbf{M}_{m,r}(\varphi_{m,r})^{\mathsf{T}} \\ &\quad \times \mathbf{W}_N\mathbf{A}_{m,r}^{(\mathrm{RX})}, \end{aligned} \tag{18b}$$

while the time-domain analysis and synthesis window matrices are now given as

$$\mathbf{A}_{m,r}^{(\mathrm{RX})} = \mathrm{diag}\left(\begin{bmatrix}\mathbf{0}_{N_{\mathrm{L}}\times 1}\\ \mathbf{1}_{N_{\mathrm{S}}\times 1}\\ \mathbf{0}_{N_{\mathrm{T}}\times 1}\end{bmatrix}\right) \tag{19a}$$

and

$$\mathbf{S}_{m,r}^{(\mathrm{RX})} = \mathrm{diag}\left(\begin{bmatrix}\mathbf{0}_{L_{\mathrm{L},m}\times 1}\\ \mathbf{1}_{L_{\mathrm{S},m}\times 1}\\ \mathbf{0}_{L_{\mathrm{T},m}\times 1}\end{bmatrix}\right), \tag{19b}$$

respectively.

Similar to TX, the RX side discontinuous FC processing starts by segmenting the received high-rate waveform $\hat{\mathbf{x}}_{\text{FC-F-OFDM}}$ into overlapping blocks. However, now the

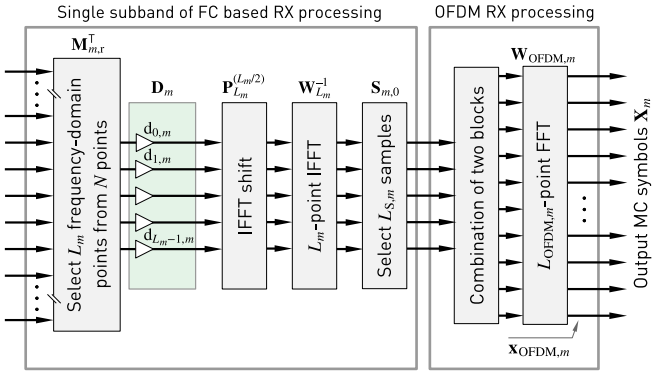

Fig. 10. Block diagram for discontinuous FC-F-OFDM receiver processing using the overlap-and-save model.

processing is carried out in blocks of length $3/2N$ as

$$\hat{\mathbf{w}}_{m,n} = \sum_{n=0}^{B_{\mathrm{OFDM},m}-1} \mathbf{\Gamma}_{\sigma_n}^{\mathsf{T}}\hat{\mathbf{x}}_{\text{FC-F-OFDM}}. \tag{20}$$

Here, it is assumed for simplicity that the length of the received waveform is Q as given by (16d) and that the waveform is synchronized such that it contains $I_m S_{\mathrm{L},m,n}$ samples before the first data symbol such that the number of zero samples inserted on the TX side and the number of samples to be removed on the RX side match. The high-rate symbols $\hat{\mathbf{w}}_{m,n}$ are further divided into two overlapping blocks of length N as

$$\hat{\mathbf{w}}_{m,n}^{(r)} = (\mathbf{R}_N^{(r)})^{\mathsf{T}}\hat{\mathbf{w}}_{m,n}, \tag{21}$$

for $r = 0, 1$. These blocks are processed by $\mathbf{G}_{m,r}(\varphi_{m,r})$'s as

$$\hat{\mathbf{z}}_{m,n}^{(r)} = \mathbf{G}_{m,r}(\varphi_{m,r})\hat{\mathbf{w}}_{m,n}^{(r)} \tag{22}$$

for $r = 0, 1$ to obtain filtered low-rate FC blocks corresponding to first and second half of the nth symbol on subband m. Finally, the filtered blocks are concatenated and the extensions are removed as

$$\hat{\mathbf{x}}_{\mathrm{OFDM},m,n} = \begin{bmatrix}\mathbf{0}_{S_{\mathrm{T},m,n}\times L_{\mathrm{OFDM},m}}\\ \mathbf{I}_{L_{\mathrm{OFDM},m}}\\ \mathbf{0}_{L_{\mathrm{T},m}\times L_{\mathrm{OFDM},m}}\end{bmatrix}^{\mathsf{T}} \sum_{r=0,1}\mathbf{R}_{L_m}^{(r)}\hat{\mathbf{z}}_{m,n}^{(r)}, \tag{23}$$

and the resulting low-rate OFDM symbol is converted back to frequency domain as a part of the OFDM demodulation process as follows:

$$\hat{\mathbf{x}}_{m,n} = \mathbf{W}_{L_{\mathrm{OFDM},m}}\hat{\mathbf{x}}_{\mathrm{OFDM},m,n}. \tag{24}$$

It is noted, that the CP part is also removed in the above processing together with the extensions due to zero padding. Alternatively, the concatenation and the removal of the extensions can be combined in

$$\hat{\mathbf{x}}_{\mathrm{OFDM},m,n} = \mathbf{P}_{L_m}^{(L_m/4)}\hat{\mathbf{z}}_{m,n}^{(0)} + \mathbf{P}_{L_m}^{(-L_m/4)}\hat{\mathbf{z}}_{m,n}^{(1)}, \tag{25a}$$

where

$$\mathbf{P}_{L_m}^{(L_m/4)} = \begin{bmatrix}\mathbf{0}_{L_m/2\times L_m/4} & \mathbf{I}_{L_m/2} & \mathbf{0}_{L_m/2\times L_m/4}\\ & \mathbf{0}_{L_m/2\times L_m} & \end{bmatrix} \tag{25b}$$

and

$$\mathbf{P}_{L_m}^{(-L_m/4)} = \begin{bmatrix}\mathbf{0}_{L_m/2\times L_m}\\ \mathbf{0}_{L_m/2\times L_m/4} & \mathbf{I}_{L_m/2} & \mathbf{0}_{L_m/2\times L_m/4}\end{bmatrix}. \tag{25c}$$

This latter form is beneficial when finding the simplified implementations for the discontinuous RX processing, as described in next section.

For clarity, it is noted that for the proposed approach, the channel estimation and equalization are carried out as for the conventional (non-filtered) CP-OFDM waveform, that is, the channel is estimated based on the known pilot or reference symbols and subcarrier-wise frequency-domain equalizer coefficients are determined based on the estimated channel.

V. Implementation Complexity

The FC processing complexity can be divided into high-rate side complexity, $C_{\text{high-rate}}$, corresponding to long FC-processing transform and low-rate (or subband-wise) complexity, $C_{\text{low-rate},m}$, corresponding to short FC-processing transform, frequency-domain windowing, and OFDM (de)modulation transform. Let us denote the FC RX processing long transform (FFT) and short transform (IFFT) complexities given in terms of number of real multiplications by $\mu(N)$ and $\mu(L_m)$, respectively, and OFDM transform (FFT) complexity by $\mu(L_{\text{OFDM},m})$.

The number of real multiplications per received data symbol can now be evaluated as

$$C_{\text{mult}} = \frac{C_{\text{high-rate}} + \sum_{m=0}^{M-1} C_{\text{low-rate},m}}{\sum_{m=0}^{M-1} L_{\text{act},m}}, \tag{26a}$$

where the high-rate and low-rate complexities per subband are defined, respectively, as

$$C_{\text{high-rate}} = \alpha\mu(N) \tag{26b}$$

and

$$C_{\text{low-rate},m} = \alpha\beta\mu(L_m) + 6\alpha L_{\text{TBW},m} + \mu(L_{\text{OFDM},m}). \tag{26c}$$

Here, $L_{\text{TBW},m}$ is the number of transition-band bins per transition band, $\alpha = 2$ is the number of FC blocks per OFDM symbol, and $\beta \leq 1$ is the implementation related factor as described in the next subsection. Factor of 6 in (26c) is due to fact that two transition bands are needed for each subband and one complex non-trivial transition-band bin requires three real multiplications in general.

For 5G NR and LTE numerologies, the minimum allocation size is one PRB corresponding to 12 subcarriers. In this case, the minimum usable FFT length for continuous processing is $L_{\text{OFDM},m} = L_m = 128$ whereas for discontinuous processing, FFT of length $L_{\text{OFDM},m} = L_m = 16$ can be used. Assuming that an efficient implementation (using split-radix algorithm) requires

$$\mu(L) = L\log_2(L) - 3L + 4 \tag{27}$$

real multiplications for transform of length L, each transform of length 128 requires $\mu(128) = 516$ real multiplications and each transform of length 16 requires $\mu(16) = 20$ real multiplications. These complexities are evaluated according to scheme requiring three real multiplications per complex multiplication as detailed in [41].

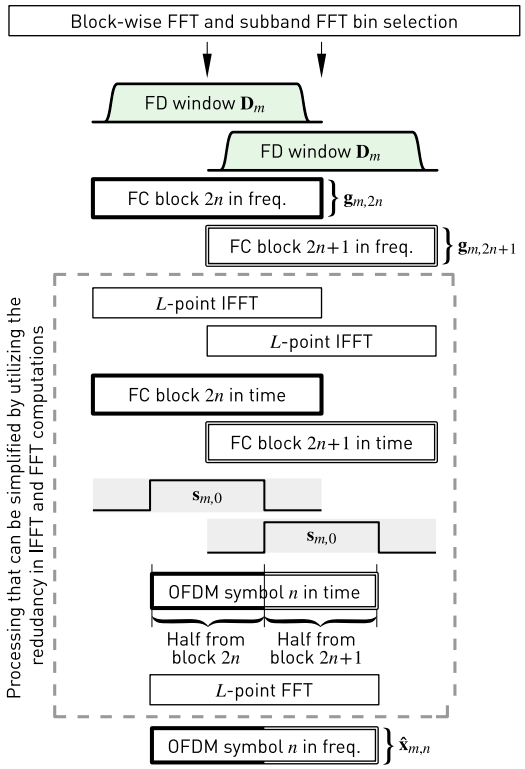

Fig. 11. Discontinuous processing for one output OFDM symbol. Dashed block represents the processing that can be simplified by sharing the IFFT computations.

A. Simplified Implementation

The basic idea for joint processing of the IFFTs of the FC-based filter and the FFT of OFDM receiver is shown in Fig. 11. This structure is made possible by the proposed symbol-synchronized discontinuous RX processing scheme.

Here, it is assumed that the length of the subband-wise OFDM symbol and the length of the IFFT used in discontinuous RX FC processing are the same $L \equiv L_{\text{OFDM},m} = L_m$. L is selected such that it contains all active SCs per subband and transition-band bins used in the frequency-domain windowing performed in the "Block-wise FFT, subband FFT bin selection and weighting" block.

For simplicity, we denote the time-domain synthesis window matrix $\mathbf{S}_{m,r}$ by $\mathbf{S}$. Now, the processing of the nth symbol from the frequency-domain FC output blocks $\mathbf{g}_{m,2n}$ and $\mathbf{g}_{m,2n+1}$ can be written as

$$\hat{\mathbf{x}}_{m,n} = \mathbf{W}_L \left[\mathbf{P}_L^{(L/4)}\mathbf{S}\mathbf{W}_L^{-1}\mathbf{g}_{m,2n} + \mathbf{P}_L^{(-L/4)}\mathbf{S}\mathbf{W}_L^{-1}\mathbf{g}_{m,2n+1}\right]. \tag{28}$$

Here, $\mathbf{P}_L^{(L/4)}$ and $\mathbf{P}_L^{(-L/4)}$ are given by (25b). Alternatively, (28) can be represented as

$$\hat{\mathbf{x}}_{m,n} = \mathbf{F}_0\mathbf{g}_{m,2n} + \mathbf{F}_1\mathbf{g}_{m,2n+1}, \tag{29a}$$

where

$$\mathbf{F}_0 = \mathbf{W}_L\mathbf{P}_L^{(L/4)}\mathbf{S}\mathbf{W}_L^{-1} \tag{29b}$$

and

$$\mathbf{F}_1 = \mathbf{W}_L\mathbf{P}_L^{(-L/4)}\mathbf{S}\mathbf{W}_L^{-1} \tag{29c}$$

are circular convolution matrices.

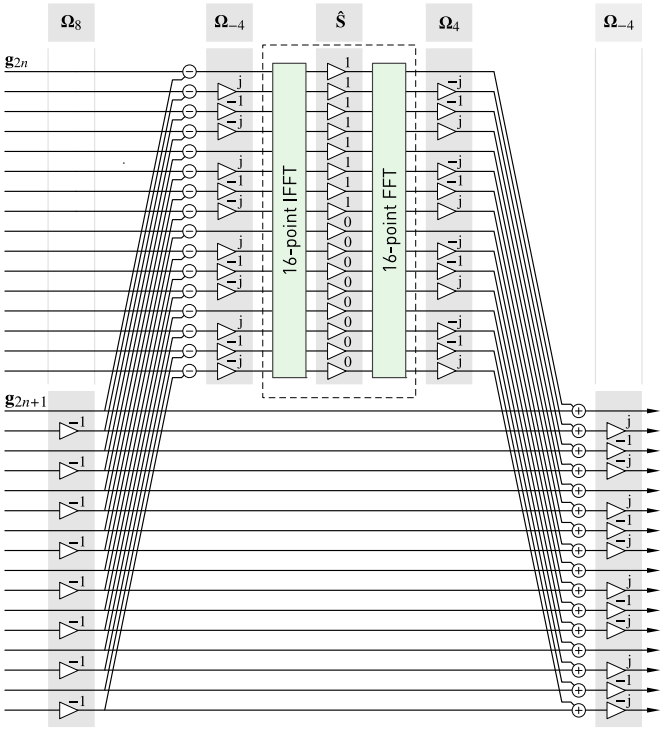

Fig. 12. Simplified discontinuous processing for $L = 16$ as described by (30). The dashed region can be further simplified by decomposing transforms into smaller transforms.

After some manipulations (28) can be reformulated as

$$\hat{\mathbf{x}}_{m,n} = \mathbf{\Omega}_{-L/4}[\mathbf{F}(\mathbf{g}_{m,2n} - \mathbf{\Omega}_{L/2}\mathbf{g}_{m,2n+1}) + \mathbf{\Omega}_{L/2}\mathbf{g}_{m,2n+1}], \tag{30a}$$

where

$$\mathbf{F} = \mathbf{\Omega}_{L/4}\mathbf{C}\mathbf{\Omega}_{-L/4} \tag{30b}$$

with

$$\mathbf{C} = \mathbf{W}_L\hat{\mathbf{S}}\mathbf{W}_L^{-1} \tag{30c}$$

and

$$\mathbf{\Omega}_\phi = \mathrm{diag}\left(\left[W_L^0\ W_L^\phi\ \cdots\ W_L^{\phi(L-1)}\right]^{\mathsf{T}}\right) \tag{30d}$$

with $W_L = \exp(-\mathrm{j}2\pi/L)$. Here, $\hat{\mathbf{S}} \in \mathbb{Z}^{L\times L}$ as given by

$$\hat{\mathbf{S}} = \mathbf{P}_L^{(L/4)}\mathbf{S}\mathbf{P}_L^{(-L/4)} \tag{30e}$$

is the time-domain synthesis window matrix circularly left and up shifted by $L/4$ samples.

The above formulation relies on rotating the $\mathbf{g}_{m,2n+1}$ and the corresponding window by $L/2$ samples. In this case, the transfer functions provided by the $\mathbf{F}_0$ and $\mathbf{F}_1$ form a lowpass-highpass filter pair essentially meaning that $\mathbf{F}_0\mathbf{F}_1 = \mathbf{I}_L$. The low-rate complexity of (30) per OFDM symbol is one IFFT and one FFT of length L as depicted in Fig. 12. The direct approach, as illustrated in Fig. 11, requires two IFFTs and one FFT of length L, that is, the saving in number of real multiplications for this simplified processing is 33.3%. In (26), $\beta = 1/2$ gives the complexity of the simplified processing whereas $\beta = 1$ gives the complexity of the direct approach. The half-band filtering provided by (30c) can be further decomposed into smaller transforms to achieve some savings in implementation, however, these decompositions are beyond the scope of this paper.

TABLE I
OPTIMIZED TRANSITION-BAND WEIGHTS

Transition-band weight	8 and 44 active SCs	624 active SCs
$\xi_m(0)$	−0.011 485 978	−0.002 130 603
$\xi_m(1)$	0.238 202 518	−0.002 679 098
$\xi_m(2)$	0.827 879 691	0.026 473 274
$\xi_m(3)$	1.010 936 145	0.128 753 910
$\xi_m(4)$		0.259 017 465
$\xi_m(5)$		0.496 440 727
$\xi_m(6)$		0.703 755 536
$\xi_m(7)$		0.846 182 217

VI. NUMERICAL RESULTS

In this section, we will analyze the performance of the discontinuous FC processing in terms of uncoded BER in different interference and channel conditions, and also show complexity comparison between continuous and discontinuous FC processing. Here we assume the overlap factor of $\lambda = 0.5$. Continuous FC processing with the overlap of $\lambda = 0.25$ marginally degrades the spectral containment and error vector magnitude (EVM) performance compared to the overlap of $\lambda = 0.5$ with the benefit of somewhat lower implementation complexity. The performance of continuous FC processing with 25% and 50% overlaps is compared in [33].

The filter transition-band weights are tabulated in Table I. The transition-band weights used by narrow-band allocations of Subsection VI.A are given by the second column while third column gives the weights for the wide-band allocations of Subsection VI.B. These transition-band weights are optimized for minimizing the in-band EVM subject to subband leakage ratio as proposed in [33]. Same transition-band weights are used for continuous and discontinuous FC processing.

The frequency-domain weights on subband m consist of two symmetric transition bands with non-trivial values $\xi_m(p)$ for $p = 0, 1, \ldots, L_{\mathrm{TBW},m} - 1$, where $L_{\mathrm{TBW},m}$ also defines the transition-band width. All passband weights are set to one and all stopband weights are set to zero, that is, the frequency-domain window is expressed as

$$\mathbf{d}_m = \begin{bmatrix} \mathbf{0}_{(\lceil\lfloor L_m - L_{\mathrm{ACT},m}\rfloor/2\rceil - L_{\mathrm{TBW},m})\times 1} \\ \xi_m(0) \\ \xi_m(1) \\ \vdots \\ \xi_m(L_{\mathrm{TBW},m}-1) \\ \mathbf{1}_{L_{\mathrm{ACT},m}\times 1} \\ \xi_m(L_{\mathrm{TBW},m}-1) \\ \xi_m(L_{\mathrm{TBW},m}-2) \\ \vdots \\ \xi_m(0) \\ \mathbf{0}_{(\lfloor\lfloor L_m - L_{\mathrm{ACT},m}\rfloor/2\rfloor - L_{\mathrm{TBW},m})\times 1} \end{bmatrix}. \tag{31}$$

TABLE II
NARROW-BAND TRANSMISSION SCENARIOS AND FILTERING CONFIGURATIONS

Channel model	Additive white Gaussian noise (AWGN)		Tapped-delay line (TDL)-C with 300 ns and 1000 ns root mean squared (RMS) channel delay spread
Synchronicity	Quasi-synchronous: No timing offset and no frequency offset between different uplink signals		Asynchronous: Timing offset of 256 samples ($L_{\mathrm{OFDM},m}/4$) between the target subband for BER evaluation and adjacent subbands on both sides
Allocated subband width	1 PRB, 12 subcarriers (SCs): 8 active SCs and 4-SC guard-bands between adjacent active subbands		4 PRBs, 48 SCs: 44 active SCs and 4-SC guardband between adjacent active subbands
Filtering configuration	OLA processing on the TX side and OLS on the RX side (if FC RX is used). The number of burst transmission is 1000 while each burst consist of 14 OFDM symbols.		
	1) No filtering on TX and RX sides	2) No TX filtering, RX filtering with continuous FC model with $L_{\mathrm{RX}} = 128$	3) Continuous TX filtering, continuous RX filtering, $L_{\mathrm{TX}} = L_{\mathrm{RX}} = 128$
	4) Discontinuous TX filtering, continuous RX filtering, $L_{\mathrm{TX}} = L_{\mathrm{RX}} = 128$	5) Discontinuous TX filtering, continuous RX filtering, $L_{\mathrm{TX}} = 16$ with 1 PRB, $L_{\mathrm{TX}} = 64$ with 4 PRBs, and $L_{\mathrm{RX}} = 128$	6) Discontinuous TX and RX filtering, $L_{\mathrm{TX}} = 16$ with 1 PRB, $L_{\mathrm{TX}} = 64$ with 4 PRBs, and $L_{\mathrm{RX}} = 128$

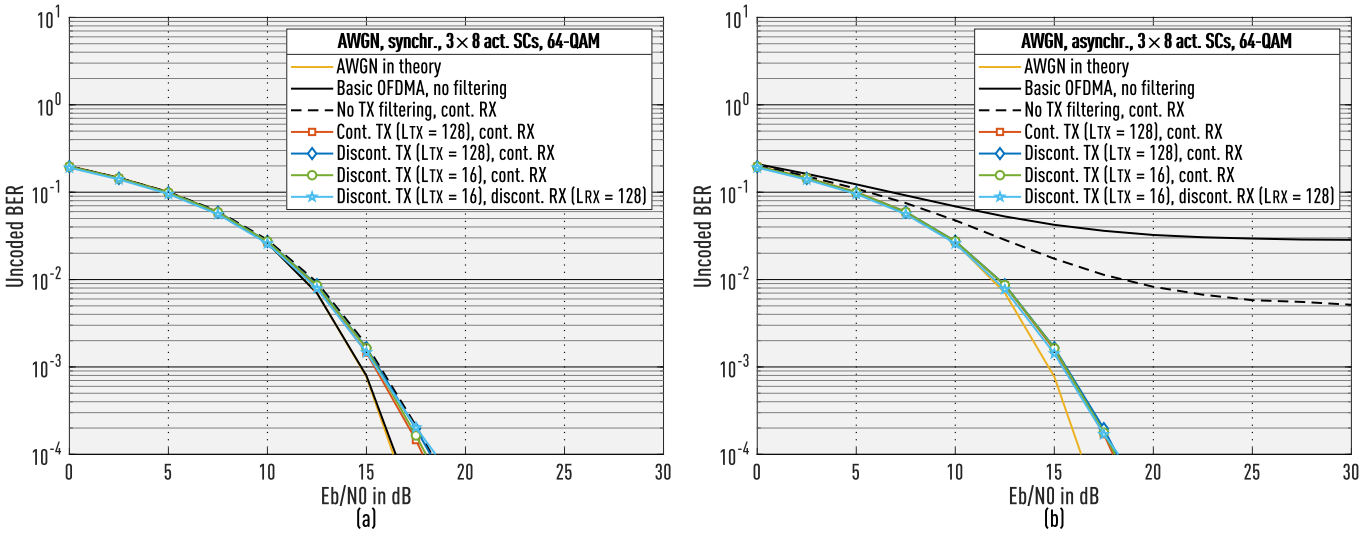

Fig. 13. Simulation results with AWGN channel and 64-QAM. (a) Quasi-synchronous cases and (b) asynchronous cases (quarter-symbol timing offset). Single PRB allocated for each of the three subbands (12 subcarriers (SCs), 8 active SCs, and 4 SCs for guardband).

TABLE III
WIDE-BAND TRANSMISSION SCENARIOS AND FILTERING CONFIGURATIONS

Channel models	AWGN and TDL-C with 1000 ns RMS channel delay spread
Synchronicity	Quasi-synchronous: No timing offset and no frequency offset between different uplink signals
Allocated subband width	52 PRBs, 624 active subcarriers (SCs) and 8-SC guardband around the active subband
Filtering configuration	1) Continuous filtering on TX and RX sides 2) Continuous TX and discontinuous RX filtering 3) Discontinuous TX and continuous RX filtering 4) Discontinuous filtering on TX and RX sides

A. Bit-Error Rate Performance in Narrow-Band Allocations

Figs. 13–16 compare the simulated uncoded BER performance of different CP-OFDM configurations, with or without subband filtering in 10 MHz 5G NR uplink scenario, with high-rate IFFT length of $N = 1024$ and SCS of 15 kHz. Table II shows details of the considered scenarios and filtering configurations. The used channel models are additive white Gaussian noise (AWGN) and tapped-delay line (TDL)-C, which is one of the channel models considered in the 5G NR development [42]. Two different values of the root-mean-squared (RMS) channel delay spread, 300 ns and 1000 ns, are used for TDL-C channel. Two subband configurations are considered: single PRB or four PRBs of 12 subcarriers. In both cases, four deactivated subcarriers are used as for guard bands. Focusing on the asynchronous up-link scenario, different instances of the channel model are always used for the three adjacent subbands included in the simulations. Perfect power control is assumed in such a way that the three adjacent subbands are always received at the same power level and constant SNR for all channel instances.

Fig. 13(a) shows the BER simulation results for AWGN channel in synchronous scenario with single PRB per subband. In this case, the performance of the TX filtered continuous and discontinuous approaches and the RX-filtering-only scheme are practically the same. When compared with the basic synchronous OFDM, the filtered schemes have a minor performance loss. In asynchronous scenario, as depicted

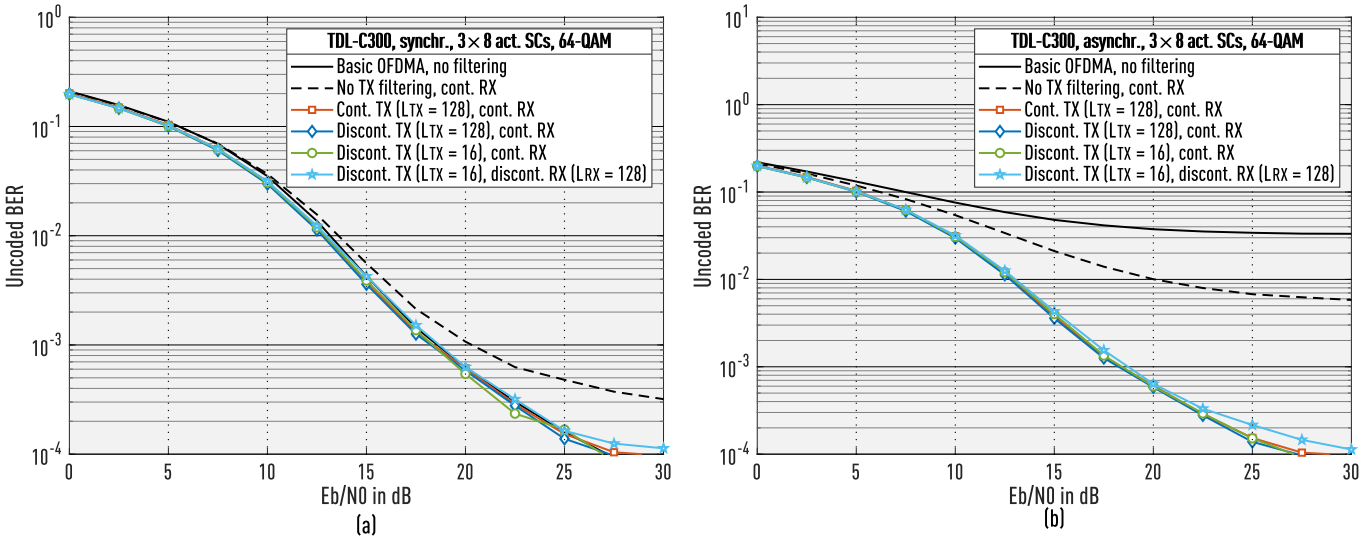

Fig. 14. Performance simulation results with TDL-C 300 ns channel and 64-QAM. (a) Quasi-synchronous cases and (b) asynchronous cases (quarter-symbol timing offset). Single PRB allocated for each subband (12 SCs, 8 active SCs, and 4 SCs for guardband).

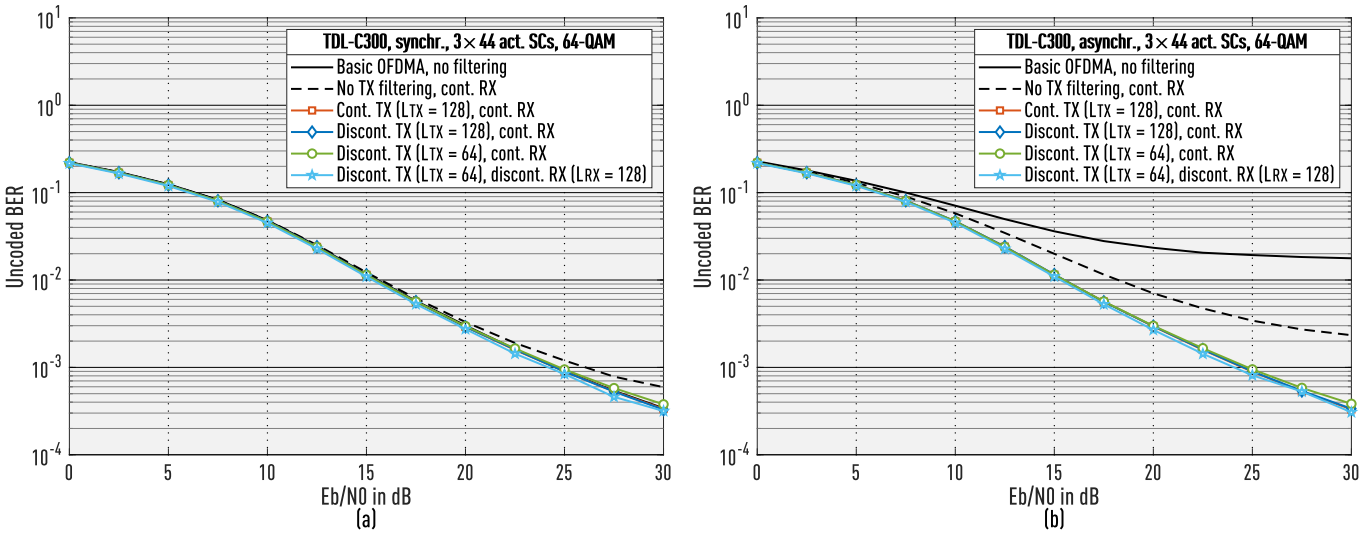

Fig. 15. Performance simulation results with TDL-C 300 ns channel and 64-QAM. (a) Quasi-synchronous cases and (b) asynchronous cases (quarter-symbol timing offset). Four PRBs allocated for each subband (48 SCs, 44 active SCs, and 4 SCs for guardband).

in Fig. 13(b), the performance of TX filtered schemes remains close to theoretical one whereas the BER floor for RX-filtering-only and basic OFDM schemes is about 0.5% and 3%, respectively. Fig. 14(a) shows the BER simulation results for TDL-C 300 ns channel in synchronous scenario with single PRB per subband. In this case, the channel maximum delay spread (about $2.6\,\mu$s) is well below the CP length (about $4.7\,\mu$s). When comparing with basic synchronous OFDM, we can see minor performance degradation of the schemes with filtering at both ends, while the degradation of the RX-filtering-only scheme is more visible. In the asynchronous case, the benefits of subband-filtered OFDM are clearly visible as illustrated in Fig. 14(b).

Fig. 15(a) compares the performance for TDL-C 300 ns channel in synchronous scenario with four PRBs per subband. Now the performance difference between the schemes has been decreased due to the fact that, on the average, the wider subbands suffer less from the interference between the subbands. The same trend can also be seen from simulation results of asynchronous scenario as shown in Fig. 15(b) where the performance degradation of RX-filtering-only and basic OFDM schemes is less obvious.

Fig. 16(a) shows the BER simulation results for TDL-C 1000 ns channel with single PRB per subband. In this case the channel maximum delay spread (about $8.7\,\mu$s) exceeds the CP duration (about $4.7\,\mu$s), resulting in higher error floor in all configurations. The same conclusions can be made as above, except that the TX filtered schemes have now better performance than the basic OFDM. The performance degradation of basic OFDM scheme is due to the inter-carrier interference (ICI) induced by the increased frequency dispersion of the channel whereas, for TX filtered OFDM, the better spectral containment provides also better protection against the ICI [43], [44]. For asynchronous scenario, as illustrated in Fig. 16(b), the performance of TX filtered schemes are approximately the same as in synchronous scenario whereas

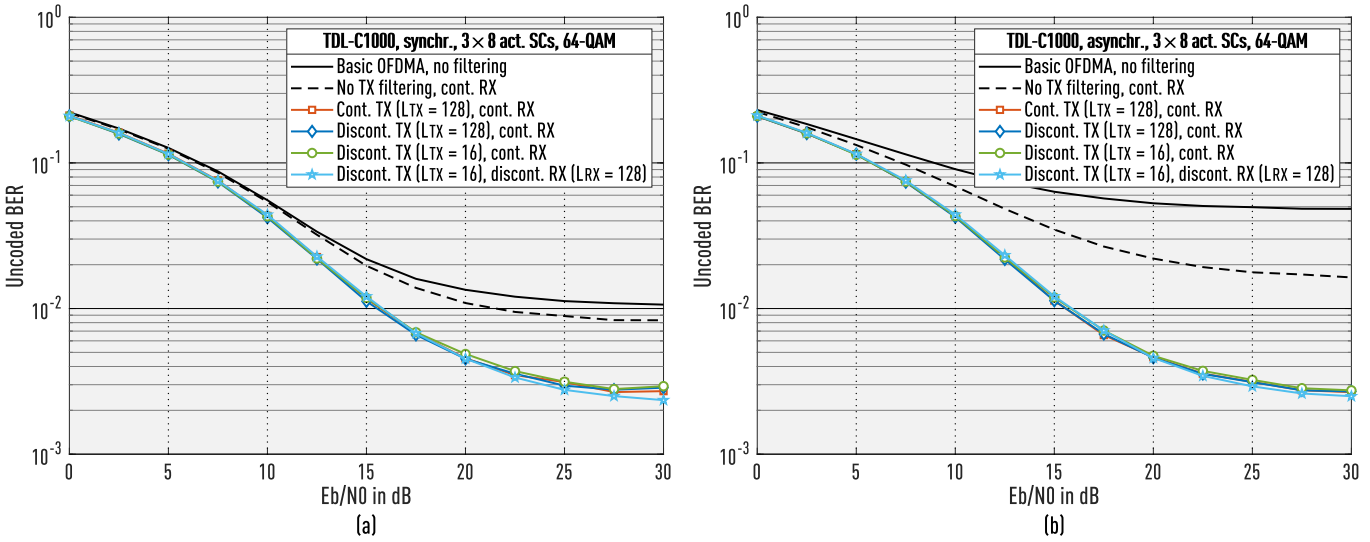

Fig. 16. Performance simulation results with TDL-C 1000 ns channel and 64-QAM. (a) Quasi-synchronous cases and (b) asynchronous cases (quarter-symbol timing offset). Single PRB allocated for each subband (12 SCs, 8 active SCs, and 4 SCs guardband).

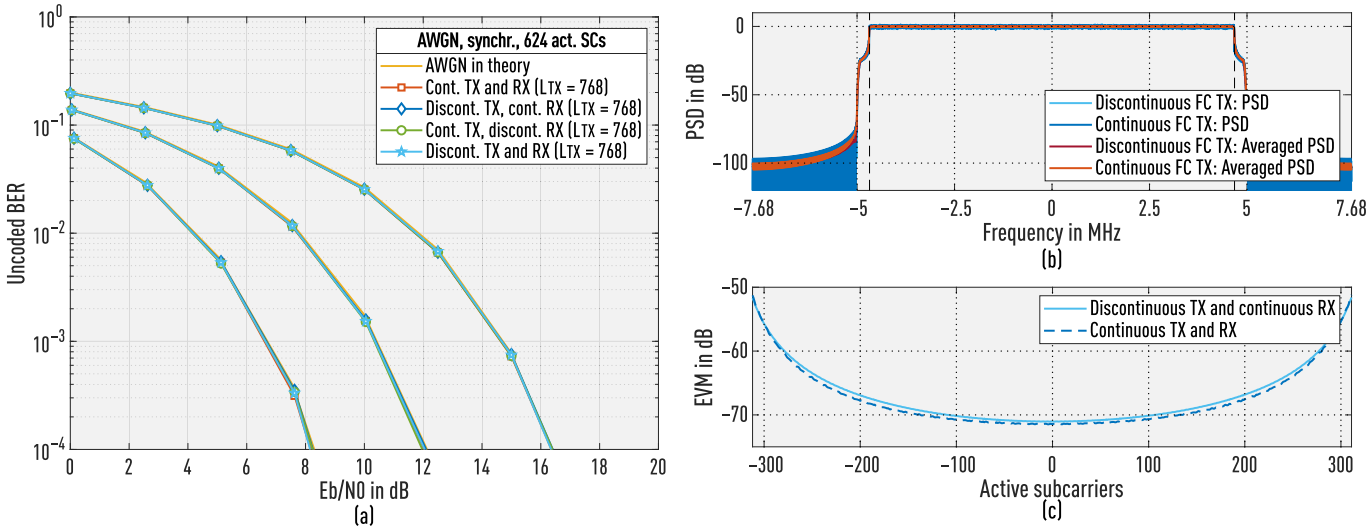

Fig. 17. (a) Performance simulation results with AWGN channel and QPSK, 16-QAM, and 64-QAM. The number of PRBs allocated for single subband is 52 (624 active SCs and 8 SCs for guardband). (b) Power spectral densities for continuous and discontinuous processing. In-band region (active subcarriers) is denoted by the vertical dashed lines. (c) Error-vector magnitude on active subcarriers with 64-QAM modulation.

the basic OFDM and RX-filtering-only schemes have considerably higher error floors than the synchronous cases. The performance improvement of the FC filtered waveforms in TDL-C 1000 ns channel remain consistent with other results.

B. Bit-Error Rate Performance in Wide-Band Allocations

Fig. 17 compares the simulated uncoded BER performance of continuous and discontinuous subband filtering in 10 MHz 5G NR uplink scenario, with high-rate IFFT length of $N = 1024$ and SCS of 15 kHz. Single subband configuration is considered with 52 active PRBs of 12 subcarriers. In this case, eight non-active subcarriers are used as for transition bands. Table III shows details of the considered scenarios and filtering configurations. The used channel models are AWGN and TDL-C.

Fig. 17(a) shows the uncoded BER for QPSK, 16-QAM, and 64-QAM. As seen from this figure, both the continuous and discontinuous processing reach the theoretical BER performance in AWGN channel. The PSDs, as illustrated in Fig. 17(b), show that both the continuous and discontinuous processing have approximately the same spectral containment. The average in-band EVM values, as shown in Fig. 17(c), are 63.5 dB and 63.3 dB for continuous and discontinuous processing, respectively.

The performance of all the unfiltered and filtered schemes are approximately the same in TDL-C channel with 300 ns delay spread. However, for channel model with maximum delay spread exceeding the CP duration, the pulse shaping provided by the filtering gives slightly improved performance over the plain CP-OFDM waveform.

C. Implementation Complexity

Figs. 18 and 19 compare the computational complexity of different FC-based filtered OFDM schemes for different subband configurations, again in the 10 MHz 5G NR or LTE

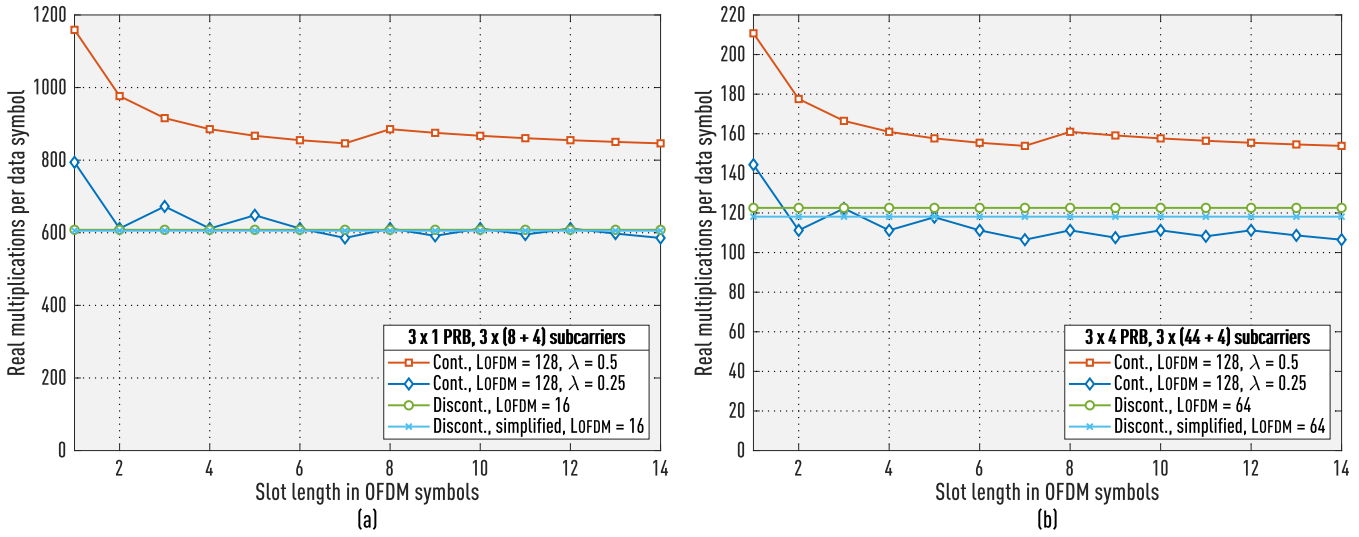

Fig. 18. Computational complexity of continuous FC-F-OFDM RX processing with 25% and 50% overlaps and discontinuous FC-F-OFDM RX processing with 50% overlap. (a) Three 1-PRB wide subbands. (b) Three 4-PRB wide subband.

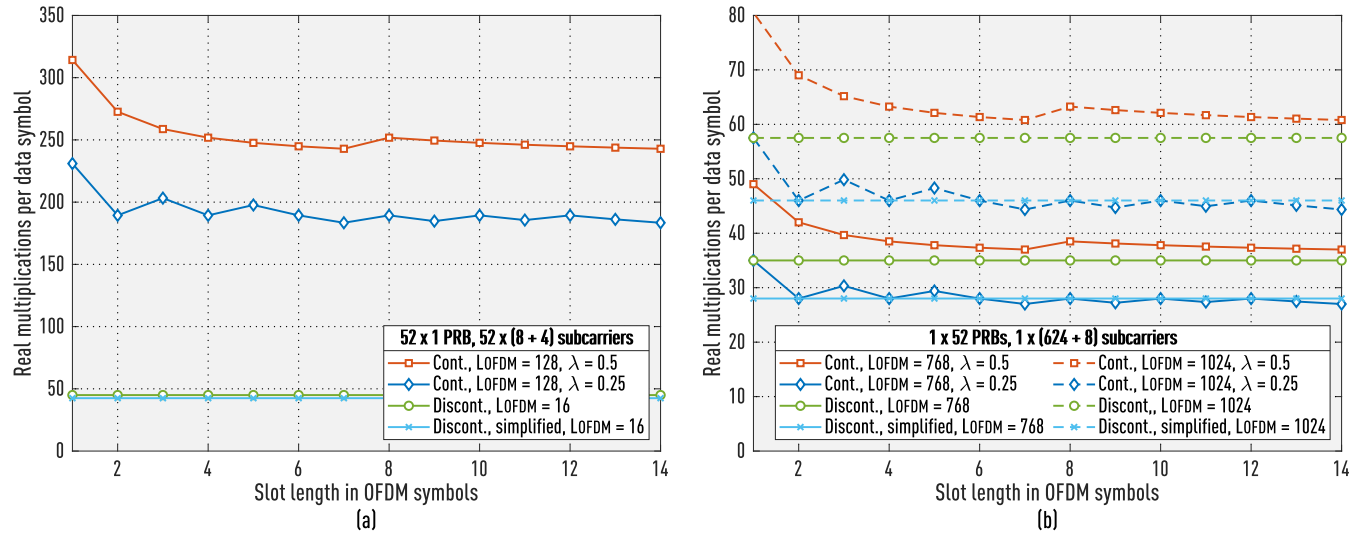

Fig. 19. Computational complexity of continuous FC-F-OFDM RX processing with 25% and 50% overlaps and discontinuous FC-F-OFDM RX processing with 50% overlap. (a) 52 1-PRB wide subbands. (b) Single 52-PRB wide subband.

case. The overlap factors of $\lambda = 0.25$ and $\lambda = 0.5$ are used for continuous processing, and $\lambda = 0.5$ for discontinuous processing. The complexity is plotted as a function of the slot (TX burst) length, in the range from 1 to 14 OFDM symbols, using the number of real multiplications per transmitted QAM symbol as the complexity metric.

The short FC-transform length L_m is equal to the IFFT length in OFDM generation and it is selected as the smallest feasible power-of-two value. Notably, the smallest value of L_m in continuous processing is 128, while in discontinuous processing we can use $L_m = 16$ for single PRB ($L_{\text{act},m} = 12$ subcarriers) allocation and $L_m = 64$ for four-PRB ($L_{\text{act},m} = 48$ subcarriers) allocation. In addition to the 1-PRB and 4-PRB subband cases, also the fullband allocation with 52 PRBs and $L_{\text{act},0} = 624$ active subcarriers is included in the comparison.

From Figs. 18 and 19, we can observe the following:

1) Discontinuous processing for all parameterizations and slot lengths provides lower complexity than continuous processing with 50% overlap. Discontinuous processing also provides constant complexity over different slot lengths. With short slot lengths, the complexity of discontinuous schemes is significantly lower than that of continuous transmission with 50% overlap.
2) With multiple relatively narrow subbands, this benefit is pronounced and significant also for higher slot lengths. In these cases, the complexity of discontinuous processing is lower or similar to that of the continuous processing with 25% overlap.
3) We remind that with 50% overlap, the imperfections of FC processing can be ignored, while the use of 25% overlap degrades the performance with high modulation and coding schemes (MCSs).
4) The use of non-power-of-two short transform length (L) in building the CP-OFDM symbols and FC processing blocks may give significant complexity reduction in both continuous and discontinuous FC processing, especially in the channel filter use case. This is shown for the

full-band transmission case with $L = 768$ instead of $L = 1024$ (channel filtering example). This transform length can be efficiently implemented by three FFTs of length 256 and some additional twiddle factors.

5) Discontinuous processing allows to generate a single-PRB subband signal (e.g. for NB IoT) by using the FFT length of 16 for the OFDM symbol generation and FC processing at the input sampling rate of 240 kHz, while prior art implementation require sampling rate of 1.92 MHz with the FFT length of 128.

The complexity evaluations for time-domain filtered OFDM and WOLA schemes and their relative complexity with respect to continuous FC processing are given in [33], [37].

VII. Conclusion

In this article, discontinuous symbol-synchronized fast-convolution (FC) processing technique was proposed, with particular emphasis on the physical layer processing in 5G-NR and beyond mobile radio networks. The proposed processing approach was shown to offer various benefits over the basic continuous FC scheme, specifically in terms of reduced complexity and latency as well as increased parameterization flexibility. The additional in-band distortion effects, stemming from the proposed scheme, were found to have only a very minor impact on the link-level performance. The benefits are particularly important in specific application scenarios, like transmission of single or multiple narrow subbands, or in mini-slot type transmission, which is a core element in the ultra-reliable low-latency transmission service of fifth-generation new radio (5G NR) networks.

Generally, discontinuous FC processing can be regarded as an additional useful element in the toolbox for frequency-domain waveform processing algorithms, and it can be useful for various other signal processing applications as well.

Acknowledgment

This article contains multimedia material, available at http://yli-kaakinen.fi/DiscontinuousSymbolSynchronizedFastConvolution/

References

[1] J. Yli-Kaakinen, T. Levanen, M. Renfors, M. Valkama, and K. Pajukoski, "FFT-domain signal processing for spectrally-enhanced CP-OFDM waveforms in 5G new radio," in *Proc. 52nd Asilomar Conf. Signals, Syst., Comput.*, Oct. 2018, pp. 1049–1056.

[2] E. Dahlman, S. Parkvall, and J. Sköld, *5G NR: The Next Generation Wireless Access Technology*. New York, NY, USA: Academic, 2018.

[3] G. Wunder *et al.*, "5GNOW: Non-orthogonal, asynchronous waveforms for future mobile applications," *IEEE Commun. Mag.*, vol. 52, no. 2, pp. 97–105, Feb. 2014.

[4] P. Banelli, S. Buzzi, G. Colavolpe, A. Modenini, F. Rusek, and A. Ugolini, "Modulation formats and waveforms for 5G networks: Who will be the heir of OFDM?: An overview of alternative modulation schemes for improved spectral efficiency," *IEEE Signal Process. Mag.*, vol. 31, no. 6, pp. 80–93, Nov. 2014.

[5] E. Memisoglu, A. B. Kihero, E. Basar, and H. Arslan, "Guard band reduction for 5G and beyond multiple numerologies," *IEEE Commun. Lett.*, vol. 24, no. 3, pp. 644–647, Mar. 2020.

[6] H. Chen, J. Hua, F. Li, F. Chen, and D. Wang, "Interference analysis in the asynchronous f-OFDM systems," *IEEE Trans. Commun.*, vol. 67, no. 5, pp. 3580–3596, May 2019.

[7] J. Mao, L. Zhang, P. Xiao, and K. Nikitopoulos, "Interference analysis and power allocation in the presence of mixed numerologies," *IEEE Trans. Wireless Commun.*, vol. 19, no. 8, pp. 5188–5203, Aug. 2020.

[8] H. A. Mahmoud and H. Arslan, "Sidelobe suppression in OFDM-based spectrum sharing systems using adaptive symbol transition," *IEEE Commun. Lett.*, vol. 12, no. 2, pp. 133–135, Feb. 2008.

[9] S. Brandes, I. Cosovic, and M. Schnell, "Reduction of out-of-band radiation in OFDM systems by insertion of cancellation carriers," *IEEE Commun. Lett.*, vol. 10, no. 6, pp. 420–422, Jun. 2006.

[10] S. Pagadarai, R. Rajbanshi, A. M. Wyglinski, and G. J. Minden, "Sidelobe suppression for OFDM-based cognitive radios using constellation expansion," in *Proc. IEEE Wireless Commun. Netw. Conf.*, Las Vegas, NV, USA, Mar./Apr. 2008, pp. 888–893.

[11] K. Panta and J. Armstrong, "Spectral analysis of OFDM signals and its improvement by polynomial cancellation coding," *IEEE Trans. Consum. Electron.*, vol. 49, no. 4, pp. 939–943, Nov. 2003.

[12] G. Kongara, C. He, L. Yang, and J. Armstrong, "A comparison of CP-OFDM, PCC-OFDM and UFMC for 5G uplink communications," *IEEE Access*, vol. 7, pp. 157574–157594, 2019.

[13] I. Cosovic, S. Brandes, and M. Schnell, "Subcarrier weighting: A method for sidelobe suppression in OFDM systems," *IEEE Commun. Lett.*, vol. 10, no. 6, pp. 444–446, Jun. 2006.

[14] H.-M. Chen, W.-C. Chen, and C.-D. Chung, "Spectrally precoded OFDM and OFDMA with cyclic prefix and unconstrained guard ratios," *IEEE Trans. Wireless Commun.*, vol. 10, no. 5, pp. 1416–1427, May 2011.

[15] G. Dai, S. Chen, and G. Wang, "Orthogonal projection with optimized reserved subcarriers mapping for sidelobe suppression in OFDM systems," *IEEE Access*, vol. 7, pp. 29662–29671, 2019.

[16] M. Faulkner, "The effect of filtering on the performance of OFDM systems," *IEEE Trans. Veh. Technol.*, vol. 49, no. 5, pp. 1877–1884, Sep. 2000.

[17] S. Leyonhjelm and M. Faulkner, "Designing for low ISI in an OFDM modem," in *Proc. IEEE Region Conf. (TENCON)*, Melbourne, VIC, Australia, Nov. 2005, pp. 1–5.

[18] C. Muschallik, "Improving an OFDM reception using an adaptive Nyquist windowing," *IEEE Trans. Consum. Electron.*, vol. 42, no. 3, pp. 259–269, Aug. 1996.

[19] T. Weiss, J. Hillenbrand, A. Krohn, and F. K. Jondral, "Mutual interference in OFDM-based spectrum pooling systems," in *Proc. IEEE 59th Veh. Technol. Conf. (VTC-Spring)*, Milan, Italy, vol. 4, May 2004, pp. 1873–1877.

[20] N. Beaulieu and P. Tan, "On the effects of receiver windowing on OFDM performance in the presence of carrier frequency offset," *IEEE Trans. Wireless Commun.*, vol. 6, no. 1, pp. 202–209, Jan. 2007.

[21] E. Bala, J. Li, and R. Yang, "Shaping spectral leakage: A novel low-complexity transceiver architecture for cognitive radio," *IEEE Veh. Technol. Mag.*, vol. 8, no. 3, pp. 38–46, Sep. 2013.

[22] R. Zayani, H. Shaiek, X. Cheng, X. Fu, C. Alexandre, and D. Roviras, "Experimental testbed of post-OFDM waveforms toward future wireless networks," *IEEE Access*, vol. 6, pp. 67665–67680, 2018.

[23] *5G Waveform and Multiple Access Techniques*, Qualcomm Technol., San Diego, CA, USA, Nov. 2015.

[24] R. Ahmed, T. Wild, and F. Schaich, "Coexistence of UF-OFDM and CP-OFDM," in *Proc. IEEE 83rd Veh. Technol. Conf. (VTC Spring)*, May 2016, pp. 1–5.

[25] X. Zhang, M. Jia, L. Chen, J. Ma, and J. Qiu, "Filtered-OFDM–Enabler for flexible waveform in the 5th generation cellular networks," in *Proc. IEEE Global Commun. Conf. (GLOBECOM)*, Dec. 2015, pp. 1–6.

[26] R. Ahmed, F. Schaich, and T. Wild, "OFDM enhancements for 5G based on filtering and windowing," in *Multiple Access Techniques for 5G Wireless Networks and Beyond*. Cham, Switzerland: Springer, Jan. 2019.

[27] J. Li, E. Bala, and R. Yang, "Resource block filtered-OFDM for future spectrally agile and power efficient systems," *Phys. Commun.*, vol. 11, pp. 36–55, Jun. 2014.

[28] R. Zakaria and D. Le Ruyet, "A novel filter-bank multicarrier scheme to mitigate the intrinsic interference: Application to MIMO systems," *IEEE Trans. Wireless Commun.*, vol. 11, no. 3, pp. 1112–1123, Mar. 2012.

[29] R. Gerzaguet, D. Demmer, J.-B. Dore, and D. Ktienas, "Block-filtered OFDM: A new promising waveform for multi-service scenarios," in *Proc. IEEE Int. Conf. Commun. (ICC)*, Paris, France, May 2017, pp. 1–6.

[30] M. Renfors, J. Yli-Kaakinen, T. Levanen, M. Valkama, T. Ihalainen, and J. Vihriälä, "Efficient fast-convolution implementation of filtered CP-OFDM waveform processing for 5G," in *Proc. IEEE Globecom Workshops (GC Wkshps)*, San Diego, CA, USA, Dec. 2015, pp. 1–7.

[31] M. Renfors, J. Yli-Kaakinen, T. Levanen, and M. Valkama, "Fast-convolution filtered OFDM waveforms with adjustable CP length," in *Proc. IEEE Global Conf. Signal Inf. Process. (GlobalSIP)*, Washington, DC, USA, Dec. 2016, pp. 635–639.
[32] J. Yli-Kaakinen, T. Levanen, M. Renfors, and M. Valkama, "Optimized fast convolution based filtered-OFDM processing for 5G," in *Proc. Eur. Conf. Netw. Commun. (EuCNC)*, Oulu, Finland, Jun. 2017, pp. 1–6.
[33] J. Yli-Kaakinen *et al.*, "Efficient fast-convolution-based waveform processing for 5G physical layer," *IEEE J. Sel. Areas Commun.*, vol. 35, no. 6, pp. 1309–1326, Jun. 2017.
[34] J. Yli-Kaakinen, M. Renfors, and E. Kofidis, "Filtered multicarrier transmission," in *Wiley 5G Ref: The Essential 5G Reference Online*, R. Tafazolli, C.-L. Wang, and P. Chatzimisios, Eds. Hoboken, NJ, USA: Wiley, 2020, ch. 2.
[35] V. Vakilian, T. Wild, F. Schaich, S. T. Brink, and J.-F. Frigon, "Universal-filtered multi-carrier technique for wireless systems beyond LTE," in *Proc. IEEE Globecom Workshops (GC Wkshps)*, Atlanta, GA, USA, Dec. 2013, pp. 223–228.
[36] M. Renfors, X. Mestre, E. Kofidis, and F. Bader, Eds., *Orthogonal Waveforms and Filter Banks for Future Communication Systems*. New York, NY, USA: Academic, 2017.
[37] J. Yli-Kaakinen, T. Levanen, A. Palin, M. Renfors, and M. Valkama, "Generalized fast-convolution-based filtered-OFDM: Techniques and application to 5G new radio," *IEEE Trans. Signal Process.*, vol. 68, pp. 1309–1326, 2020.
[38] *Technical Specification Group Radio Access Network; Evolved Universal Terrestrial Radio Access (E-UTRA); Base Station (BS) Radio Transmission and Reception (Release 16)*, document TS 36.104 V16.2.0, 3GPP, Jun. 2019.
[39] *Technical Specification Group Radio Access Network; NR; Base Station (BS) Radio Transmission and Reception (Release 16)*, document TS 38.104 V16.0.0, 3GPP, Jun. 2019.
[40] P. P. Vaidyanathan, *Multirate Systems and Filter Banks*. Englewood Cliffs, NJ, USA: Prentice-Hall, 1993.
[41] H. Sorensen, M. Heideman, and C. Burrus, "On computing the split-radix FFT," *IEEE Trans. Acoust., Speech, Signal Process.*, vol. ASSP-34, no. 1, pp. 152–156, Feb. 1986.
[42] *Technical Specification Group Radio Access Network; Study on Channel Model for Frequency Spectrum Above 6 GHz (Release 15)*, document TR 38.900 V15.0.0, 3GPP, Jun. 2018.
[43] T. Strohmer and S. Beaver, "Optimal OFDM design for time-frequency dispersive channels," *IEEE Trans. Commun.*, vol. 51, no. 7, pp. 1111–1122, Jul. 2003.
[44] Z. Zhao, M. Schellmann, X. Gong, Q. Wang, R. Böhnke, and Y. Guo, "Pulse shaping design for OFDM systems," *EURASIP J. Wireless Commun. Netw.*, vol. 2017, no. 1, pp. 1–25, 2017.

Juha Yli-Kaakinen received the M.Sc. degree in electrical engineering and the Doctor of Technology degree (Hons.) from the Tampere University of Technology (TUT), Tampere, Finland, in 1998 and 2002, respectively.

Since 1995, he has been holding various research positions with TUT. His research interests are in digital signal processing, especially in digital filter and filter-bank optimization for communication systems and very large scale integration implementations.

AlaaEddin Loulou received the bachelor's degree in electrical engineering from the Islamic University of Gaza, Gaza, Palestine, in 2006, and the M.Sc. and D.Sc. degrees in communication engineering from Tampere University, Finland, in 2013 and 2019, respectively.

He has held various research positions with Tampere University. He is currently working as a System on Chip Engineer with Nokia Mobile Networks, Finland. His current research interests include enhanced orthogonal frequency-division multiplexing waveforms and advanced multicarrier schemes.

Toni Levanen received the M.Sc. and D.Sc. degrees from the Tampere University of Technology (TUT), Finland, in 2007 and 2014, respectively.

He is currently with the Department of Electrical Engineering, Tampere University. In addition to his contributions in academic research, he has worked in industry on wide variety of development and research projects. His current research interests include physical layer design for 5G NR, interference modeling in 5G cells, and high-mobility support in millimeter-wave communications.

Kari Pajukoski received the B.S.E.E. degree from the Oulu University of Applied Sciences in 1992. He is currently a fellow of Nokia Bell Labs. He has a broad experience from cellular standardization, link and system simulation, and algorithm development for products. He has more than 100 issued U.S. patents, from which more than 50 have been declared as standards essential patents. He is the author or coauthor of more than 300 standards contributions and 30 publications, including conference proceedings, journal contributions, and book chapters.

Arto Palin received the M.Sc.(Tech.) degree from the Tampere University of Technology. He is currently working as the Technical Leader with Nokia Mobile Networks, Finland, in the area of 5G SoC architectures. He has long industrial experience in wireless technologies, covering cellular networks, broadcast systems, and local area communications.

Markku Renfors (Life Fellow, IEEE) received the D.Tech. degree from the Tampere University of Technology (TUT), Tampere, Finland, in 1982.

Since 1992, he has been a Professor with the Department of Electronics and Communications Engineering, TUT, where he was the Head from 1992 to 2010. His research interests include filter-bank-based multicarrier systems and signal processing algorithms for flexible communications receivers and transmitters. He was a co-recipient of the Guillemin-Cauer Award (together with T. Saramäki) from the IEEE Circuits and Systems Society in 1987.

Mikko Valkama (Senior Member, IEEE) received the D.Sc.(Tech.) degree (Hons.) from the Tampere University of Technology, Finland, in 2001. In 2003, he was with the Communication Systems and Signal Processing Institute, SDSU, San Diego, CA, USA, as a Visiting Research Fellow. He is currently a Full Professor and the Department Head of electrical engineering with Tampere University (TAU), Finland. His general research interests include radio communications, radio localization, and radio-based sensing, with particular emphasis on 5G and beyond mobile radio networks.